mathematics

MDPI

Article

Fixed-Time Adaptive Event-Triggered Guaranteed Performance Tracking Control of Nonholonomic Mobile Robots under Asymmetric State Constraints

Kairui Chen, Yixiang Gu, Weicong Huang, Zhonglin Zhang, Zian Wang and Xiaofeng Wang *

School of Mechanical and Electrical Engineering, Guangzhou University, Guangzhou 510006, China; kray@gzhu.edu.cn (K.C.)
* Correspondence: 105485@gzhu.edu.cn

Abstract: A fixed-time adaptive guaranteed performance tracking control is investigated for a category of nonholonomic mobile robots (NMRs) under asymmetric state constraints. For the sake of favorable transient and steady-state properties of the system, a prescribed performance function (PPF) is introduced and a transform function is further constructed. Based on the backstepping technique, an asymmetric barrier Lyapunov function is formulated to ensure the tracking errors converge within a human-specified time. On the foundation of this, the occupation of communication channel is effectively reduced by assigning an event-triggered mechanism (ETM) with relative threshold to the process of controller design. By utilizing the proposed control strategy, the NMR is capable of implementing the enemy dislodging mission while the enemy can always be caught by the NMR and the collision would never be presented. Finally, two simulation experiments are given to verify the effectiveness of the proposed scheme.

Keywords: fixed-time control; event-triggered mechanism; asymmetric barrier Lyapunov function; prescribed performance function

MSC: 93D40

Citation: Chen, K.; Gu, Y.; Huang, W.; Zhang, Z.; Wang, Z.; Wang, X. Fixed-Time Adaptive Event-Triggered Guaranteed Performance Tracking Control of Nonholonomic Mobile Robots under Asymmetric State Constraints. *Mathematics* **2024**, *12*, 1471. https://doi.org/10.3390/math12101471

Academic Editor: Inés Tejado

Received: 3 April 2024
Revised: 2 May 2024
Accepted: 7 May 2024
Published: 9 May 2024

1. Introduction

Over the past few years, robots have been rapidly spawned into numerous varieties due to their reliability, e.g., unmanned aerial vehicles (UAVs) [1,2], autonomous underwater vehicles (AUVs) [3,4], humanoid robots [5,6], etc. Among them, wheeled mobile robots (WMRs) are considered some of the most promising robots on account of their outstanding dynamic performance and simple mechanism structure [7]. It is worth pointing out that MWRs are also known as nonholonomic mobile robots (NMRs) due to the nonholonomic constraint, meaning the robot can only move along the vertical direction of the axis of the two propelling wheels [8]. Therefore, NMRs could have more total degrees of freedom than controllable degrees of freedom, and it is possible for NMRs to track various kinds of trajectories between two arbitrary setpoints when the transverse slides are ignored.

Practically, the nonholonomic constraint brings difficulties to the controller design for the stabilization of NMRs, since the system does not satisfy Brockett's theorem [9]. Therefore, it cannot be stabilized to the desired state by utilizing a differentiable or continuous state-feedback controller, which attracts a great many scholars to investigate the tracking control for NMRs [10–15]. In Ref. [10], to ensure the steady-state performance, a finite-time control for NMRs with input and state constraints was proposed based on neural network and dynamic surface techniques. In Ref. [11], with a linearization feedback technique, tracking control for NMRs was studied to get rid of the stabilization problem caused by the optimization of model predictive control. In Ref. [12], utilizing terminal sliding mode method, an adaptive fast dynamic control strategy for NMRs was developed, which avoids

the singularity problem from being presented in the controller. Ref. [13] developed a state or output-feedback tracking controller for NMRs with uncertain disturbances and achieved the finite-time convergence of tracking errors. In Ref. [14], motion control of NMRs was proposed at the actuator level to guarantee the performance of trajectory tracking. However, most of the aforementioned literature has not take other constraints presented in practical applications into account, which are of significance to be studied.

At the same time, state constraint is widely available in some practical applications for NMRs, for instance, dislodging an enemy. It is required that the robot should maintain visibility with the enemy, but should not have a collision with it [16,17]. Usually, to handle the above two state constraints, which can be divided into symmetric and asymmetric constraints, scholars introduced the barrier Lyapunov functions (BLFs) to the controller design for NMRs [18–21]. For the symmetric constraints, in Ref. [18], the BLF was established to handle the state constraints issue for nonlinear control-affine systems to guarantee asymptotical stabilization. Ref. [19] introduced BLF into a formation controller designing process to cope with the state constraints problem presented between leaders and followers. For asymmetric constraints, in Ref. [20], a tracking control was proposed for strict-feedback nonlinear systems by constructing an asymmetric barrier Lyapunov function (ABLF), which solves the tracking issues of constrained systems without altering the controller structure. Ref. [21] developed a ABLF-based robust adaptive attitude controller for a hypersonic flight vehicle to limit the angle of attack constraint to be in a human-specified asymmetric range. Theoretically, these methods make contributions to the finite-time or asymptotical convergence of the tracking control problem for NMRs, but the NMRs require shorter and certain convergence time in practical engineering.

Nevertheless, the convergence time of finite-time or Lyapunov stabilization control framework would be impacted by the initial conditions of the system, meaning the convergence time of the system is usually unpredictable when the initial conditions change [22]. To guarantee the convergence time of the system, fixed-time control methods have been proposed and extensively reported [23–27]. In Ref. [23], a multivariable fixed-time formation control scheme based on a fixed-time disturbance observer was investigated to overcome the difficulties from multiple uncertainties of the NMRs. Ref. [24] proposed a distributed observer-based fixed-time consensus control strategy for NMRs with directed switching topologies. In Ref. [25], for a type of second-order multi-agent system subjected to actuator failures, a practical robust fixed-time containment control protocol was developed. In Ref. [26], for high-order systems, a fixed-time and singularity-free controller was established for missile guidance by utilizing terminal sliding mode strategy. Nonetheless, how to guarantee both the transient and steady-state performance of the tracking errors and convergence within a predefined time for the tracking control of the NMRs under the mentioned asymmetric constraints is a meaningful interest of research.

In actual network control, limited network bandwidth should also be considered, as it may deteriorate the control performance, because high-frequency data transmission would make the communication channel congested. Compared with a classical time-triggered mechanism, an event-triggered mechanism (ETM) was proposed to preserve the communication bandwidth, which has attracted the attention of numerous scholars [28–31]. In Ref. [28], a dynamic ETM consensus control protocol for multi-agent systems was proposed to achieve consensus asymptotically and make the triggered instants more reasonable. Ref. [29] investigated an ETM-based neural network control scheme and effectively restrained vibration in flexible structures. Ref. [30] addressed the stabilization and compensated time-delay for large-scale interconnected systems by constructing an ETM-based controller with a backstepping method. Furthermore, Refs. [32,33] combined the ETM with adaptive control strategy for mobile robots, aimed at handling the unavailable parameters of the robot while the communication bandwidth was effectively saved. Undoubtedly, the aforementioned literature has made great contributions on ETM control in different domains, but it is remaining a challenging issue to reach adaptive fixed-time convergence under limited communication resources.

Inspired by the above discussions, a fixed-time adaptive event-triggered tracking control with guaranteed performance is investigated for NMRs under asymmetric state constraints in this research. The major contributions of this study are as follows:

1. To guarantee the transient and steady-state performance of system, PPF and ABLF are both introduced into the process of backstepping design. Therefore, the violation of asymmetric state constraints is effectively prevented. Specifically, the NMR shows great tracking performance since the collision between enemy robot and NMR is avoided throughout the dislodging mission and the NMR never loses the visibility of the enemy.
2. Compared with the finite-time control scheme in Refs. [10,12,13], a fixed-time event-triggered convergence of the system is implemented by utilizing the proposed method, for which the upper boundary of convergence time is not impacted by different initial conditions. Concretely, by utilizing the proposed method, the NMR can track the enemy in a given period and implement the mission under limited communication resources. At the same time, the Zeno phenomenon is effectively avoided.

The remainder of the research is divided into following four sections. Section 2 introduces the kinetic model of the system and some preliminaries. In Section 3, the process of control method design and stability analysis are investigated. Section 4 verifies the validity of the mentioned method through some simulations examples. The conclusion is provided in Section 5.

2. System Description and Preliminaries

2.1. System Description

A class of NMRs comprising two propelling wheels and one passive wheel, whose transverse slide and force are ignored, can be described as follows [15,17]:

$$\begin{aligned} \dot{\eta} &= J(\eta)\omega^* \\ M\dot{\omega}^* &= -C(\dot{\eta})\omega^* - D\omega^* + U \end{aligned} \tag{1}$$

where $\eta = [x, y, \phi]^T$ represents the posture of the robots, which consists of the position (x, y) and the orientation angle ϕ in the earth-fixed rectangular coordinate system, $\omega^* = [\varpi_1, \varpi_2]^T$ is the angular velocity of the two wheels, $U = [u_1, u_2]$ stands for the control torque input applied to the two wheels, M is a symmetric positive-definite inertia matrix, $C(\dot{\eta})$ denotes the centripetal and Coriolis matrix, and D is the damping matrix. The matrices $J(\eta), M, C(\dot{\eta})$, and D in a dynamic system (1) are expressed by:

$$J(\eta) = \frac{r}{2}\begin{bmatrix} \cos\phi & \cos\phi \\ \sin\phi & \sin\phi \\ b^{-1} & -b^{-1} \end{bmatrix}, M = \begin{bmatrix} m_1 & m_2 \\ m_2 & m_1 \end{bmatrix}, C(\dot{\eta}) = \begin{bmatrix} 0 & c\dot{\phi} \\ c\dot{\phi} & 0 \end{bmatrix}, D = \begin{bmatrix} d_1 & 0 \\ 0 & d_2 \end{bmatrix}$$

where r and b represent the radius of the wheels and half width of the robots, respectively. All of the system parameters m_1, m_2, b, r, centripetal and Coriolis coefficient c, and damping coefficient d_1, d_2 are supposed to be the unknown constants.

For facilitation, the angular velocities of two wheels ϖ_1, ϖ_2 are converted into the linear velocity v and angular velocity ϖ of the robots as the following equation:

$$v^* = B^{-1}\omega^* \tag{2}$$

where $v^* = [v, \varpi]^T$, $B = \frac{1}{r}\begin{bmatrix} 1 & b \\ 1 & -b \end{bmatrix}$. The matrix B is invertible and satisfies $\det(B) = -\frac{2b}{r}$.

Next, substituting (2) into system (1), the transformed dynamic equation of the robotic system can be obtained as follows:

$$\begin{aligned} \dot{x} &= v\cos\phi \\ \dot{y} &= v\sin\phi \\ \dot{\phi} &= \varpi \\ \dot{v} &= m_v(\beta_v + u_v) \\ \dot{\varpi} &= m_\varpi(\beta_\varpi + u_\varpi) \\ \dot{x}\sin\phi - \dot{y}\cos\phi &= 0 \end{aligned} \tag{3}$$

where $m_v = \frac{r}{2(m_1+m_2)}, m_\varpi = \frac{r}{2(m_1-m_2)}, \beta_v = \frac{2bc\varpi^2}{r} - \frac{v(d_1+d_2)}{r} - \frac{b\varpi(d_1-d_2)}{r}, \beta_{\varpi,j} = -\frac{2vc\varpi}{r} - \frac{v(d_1-d_2)}{r} - \frac{b\varpi(d_1+d_2)}{r}, u_v = u_1 + u_2$, and $u_\varpi = u_1 - u_2$.

2.2. Relative Posture Constraints [34]

In this work, one of the objectives is to develop a prescribed performance controller that enables a NMR to implement a task for dislodging an enemy in a certain trajectory and satisfy desired relative distance and direction constraints simultaneously.

The desired trajectory for the dislodged enemy can be generated by the following dynamic equation:

$$\begin{aligned} \dot{x}_d &= v_d\cos\phi_d \\ \dot{y}_d &= v_d\sin\phi_d \\ \dot{\phi}_d &= \varpi_d \end{aligned} \tag{4}$$

where v_d and ϖ_d are the linear velocity and angular velocity of the target enemy, respectively. The desired posture of the enemy robot can be expressed as $\eta_d = [x_d, y_d, \phi_d]^T$.

Assuming the relative distance and direction between the robot and the target enemy should always fall into a given range, we considered the following limitations: tracking range constraint, collision avoidance constraint, and bearing angle constraint.

Remark 1. *In some actual tracking applications for NMRs, for example, dislodging an enemy, it is required that the robot should maintain visibility to the enemy via its equipped cameras or sensors, but it should not have a collision on the enemy. On the one hand, if the enemy escapes away from the robot's practical visible area, it would be challenging to proceed with the dislodging mission. On the other hand, it is disastrous for the robot to crash against the enemy while carrying out dislodging, which probably leads to physical damage, performance deterioration, or even loss of control. Therefore, in this work, the aforementioned dislodging mission is considered, and it is of great necessity for NMRs to ensure that the relative distance and bearing angle constraints are never violated.*

2.2.1. Tracking Range Constraint

By utilizing plane coordinate transformation, we introduce the posture error equation between the robot and the enemy as follows:

$$\begin{bmatrix} \tilde{x} \\ \tilde{y} \\ \tilde{\phi} \end{bmatrix} = \begin{bmatrix} \cos\phi & \sin\phi & 0 \\ -\sin\phi & \cos\phi & 0 \\ 0 & 0 & 1 \end{bmatrix} \begin{bmatrix} x_d - x \\ y_d - y \\ \phi_d - \phi \end{bmatrix} \tag{5}$$

The relative distance $e_v(t)$ and bearing angle $e_\varpi(t)$ between the robot and the target enemy are defined by the following equations, respectively:

$$e_v(t) = \sqrt{(x - x_d)^2 + (y - y_d)^2} \tag{6}$$

$$e_\varpi(t) = arc\tan 2(\tilde{y}, \tilde{x}) \tag{7}$$

where $arc\tan 2(\tilde{y},\tilde{x}) \in (-\pi,\pi]$ is the arctangent function of the two parameters $(\tilde{x},\tilde{y})$ and returns the appropriate interior angle e_ϖ of the point $(\tilde{x},\tilde{y})$, as shown in Figure 1a.

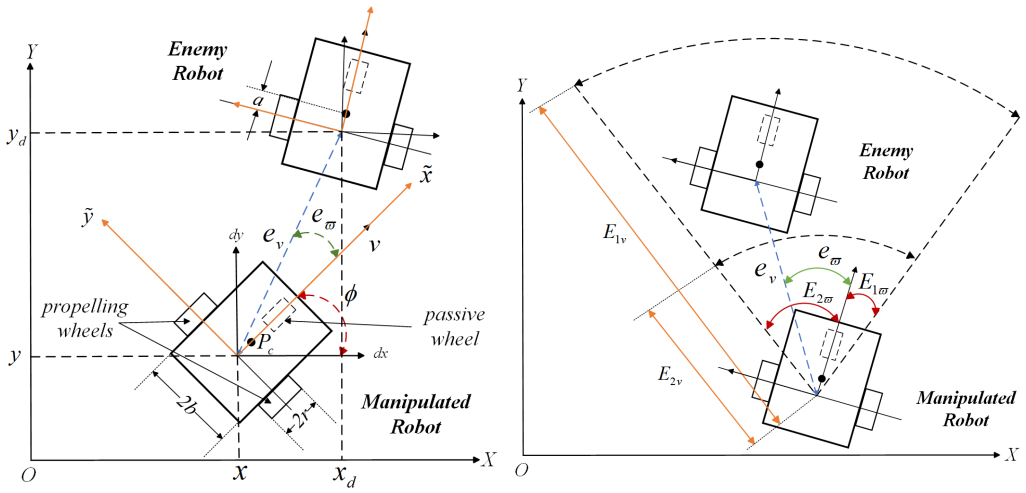

(**a**) basic setup (**b**) relative posture constraints

Figure 1. diagrams of the enemy robot and the manipulated robot in a dislodging mission.

The following tracking range constraint is taken into account:

$$e_v(t) < E_{1v} \tag{8}$$

where E_{1v} represents reliable tracking range predefined as the acceptable maximal distance to sustain the dislodgement between the robot and the enemy. That is, inequality (8) should never be violated so that the dislodgement can continue to proceed.

2.2.2. Collision Avoidance Constraint

Consider the collision avoidance constraint:

$$e_v(t) > E_{2v} \tag{9}$$

where E_{2v} represents the safety distance between the robot and the target, which is related to the volume of the robot and predefined as the minimal distance between the above two objects to avoid collision. Thus, if inequality (9) can be always satisfied, the robot is collision free.

2.2.3. Bearing Angle Constraint

In addition to the above relative distance constraints, relative angle constraint, in other words, bearing angle constraint, is also considered, which is proposed from the controller singularity problem caused by robot's nonholonomic constraint. The bearing angle between the robot and the enemy is restricted by the following constraint:

$$E_{2\omega} < e_\omega(t) < E_{1\omega} \tag{10}$$

where $0 < E_{1\omega} < \frac{\pi}{2}$ and $-\frac{\pi}{2} < E_{2\omega} < 0$ are the maximal and minimal bearing angles between the robot and the enemy, respectively.

To guarantee the relative distance and direction constraints proposed in (8) and (9) would not be violated, the desired relative distance $\bar{E}_v$ and the bearing angle $\bar{E}_\omega$ are introduced. Thus, the tracking error system is defined as follows:

$$\begin{aligned} z_v(t) &= e_v(t) - \bar{E}_v \\ z_\omega(t) &= e_\omega(t) - \bar{E}_\omega \end{aligned} \tag{11}$$

where $\bar{E}_v$ and $\bar{E}_\varpi$ represent specified values, satisfying desired relative distance and bearing angle, respectively.

The above constraints would be converted to the constrained tracking control problem if the error system (11) is limited to the following inequalities for:

$$E_{2v} - \bar{E}_v < z_v < E_{1v} - \bar{E}_v \tag{12}$$

$$-E_\varpi - \bar{E}_\varpi < z_\varpi < E_\varpi - \bar{E}_\varpi \tag{13}$$

2.3. Prescribed Performance Function [35]

To restrict the error system into a specified region for better convergence performance of $z_v(t)$ and $z_\varpi(t)$, the PPF is introduced as follows:

$$B_i(t) = (B_i(0) - B_i(\infty))e^{-\chi_i t} + B_i(\infty)(i = v, \varpi) \tag{14}$$

where $B_i(t)$ is an exponentially decaying function of time, χ_i represents a designed positive-definite constant relating to the decaying speed of $B_i(t)$, and $B_i(0)$ and $B_i(\infty)$ denote the initial value and the final value of $B_i(t)$, respectively. Prescribed performance requirement of the error system is expressed as follows:

$$\begin{array}{l} B_{1v}(t) < z_v(t) < B_{2v}(t) \\ B_{1\varpi}(t) < z_\varpi(t) < B_{2\varpi}(t) \end{array} \tag{15}$$

We assume that existing parameters λ_i, λ_i, and Q_i satisfy the inequalities $\lambda_i < B_i(0)$, $\lambda_i Q_i^{-1} < B_i(\infty)$, $\lambda_i < B_i(0)$, and $\lambda_i Q_i^{-1} < B_i(\infty)$. Thus, the transform function $l_i(t)$ is constructed as follows:

$$l_i(t) = \frac{e^{\chi_i(t)}}{(1 - Q_i^{-1}) + Q_i^{-1} e^{\chi_i(t)}} \tag{16}$$

Note that the inequalities $\lambda_i l_i^{-1}(t) \leq B_i(t)$ and $\lambda_i l_i^{-1}(t) \leq B_i(t)$ always hold; they are very important for the following deductions and proofs.

For convenience, $e(t)$, $z(t)$, $B(t)$, and $l(t)$ will be rewritten as e, z, B, and l, respectively, in the following analyses.

2.4. Preliminaries

Lemma 1 ([29]). *In view of following dynamical system:*

$$\dot{x} = f(x) \tag{17}$$

where $f(x)$ is a continuous function, $x \in \mathbb{R}^n$ represents the state vector and $x(0) = 0, f(x) = 0$. If there exists a positive-definite function $V(x)$ which satisfies:

$$\dot{V}(x) \leq -\gamma_1 V(x)^p - \gamma_2 V(x)^q + \Lambda \tag{18}$$

where $\gamma_1 > 0, \gamma_2 > 0, \Lambda > 0, p \in (1, \infty), q \in (0, 1)$. The origin of the system (17) is practically fixed-time stable, and the convergence time T is given as follows:

$$T \leq \frac{1}{\gamma_1 \kappa (p-1)} + \frac{1}{\gamma_2 \kappa (1-q)} \tag{19}$$

where $0 < \kappa < 1$. Moreover, the solution of the system can converge to:

$$\delta = \left\{ x | V(x) \leq \min\left\{ \left(\frac{\Lambda}{(1-\kappa)\gamma_1} \right)^{\frac{1}{p}}, \left(\frac{\Lambda}{(1-\kappa)\gamma_2} \right)^{\frac{1}{q}} \right\} \right\} \tag{20}$$

Lemma 2 ([19]). *For* $\forall o \in \mathbb{R}$ *and* $\forall \eta > 0$, *one has:*

$$0 \leq |o| - o\tanh\left(\frac{o}{\eta}\right) \leq 0.2785\eta \tag{21}$$

Lemma 3 ([22]). *For* $\forall a_1 \in \mathbb{R}$ *and* $\forall a_2 \in \mathbb{R}$, *one has:*

$$a_1 a_2 \leq \frac{\varepsilon^b}{b}|a_1|^b + \frac{1}{c\varepsilon^c}|a_2|^c \tag{22}$$

where $b > 1, c > 1, \varepsilon > 0$ *and,* $(b-1)(c-1) = 1$.

Lemma 4 ([36]). *For* $\alpha \in \mathbb{R}, \beta \in \mathbb{R}, m_1 > 0, m_2 > 0$, *and* $k > 0$, *one has:*

$$|\alpha|^{m1}|\beta|^{m2} \leq \frac{m_1}{m_1+m_2}k|\alpha|^{m1+m2} + \frac{m_2}{m_1+m_2}k^{-\frac{m_1}{m_2}}|\beta|^{m1+m2} \tag{23}$$

Lemma 5 ([27]). *For* $a > |z|$, $a > 0$, *and* $z \in \mathbb{R}$, *one has:*

$$\ln\frac{a^2}{a^2-z^2} \leq \frac{z^2}{a^2-z^2} \tag{24}$$

3. Controller Design and Stability Analysis

3.1. Fixed-Time Adaptive Event-Triggered Guaranteed Performance Controller Design

First, the transformation errors are defined as:

$$\begin{aligned} s_{1v} &= l_v z_v \\ s_{1\varpi} &= l_\varpi z_\varpi \end{aligned} \tag{25}$$

where l_v and l_ϖ both satisfy the definition from (16).

The error system is constructed as:

$$\begin{aligned} s_{2v} &= v - \alpha_v \\ s_{2\varpi} &= \varpi - \alpha_\varpi \end{aligned} \tag{26}$$

where α_v and α_ϖ represent the virtual controllers of v and ϖ, respectively.

Moreover, for the purpose of handling asymmetric barrier constraints, the function $q_i(s_i)(i = v, \varpi)$ is defined as:

$$q_i(s_i) = \begin{cases} 1, s_i \geq 0 \\ 0, s_i < 0 \end{cases} \tag{27}$$

Step 1. According to Equations (3), (6), (7), and (11), the derivatives of z_v and z_ϖ can be expressed as follows:

$$\begin{aligned} \dot{z}_v &= -v\cos e_\varpi + v_d\cos\theta \\ \dot{z}_\varpi &= -\varpi + \frac{v}{e_v}\sin e_v - \frac{v_d}{e_v}\sin\theta \end{aligned} \tag{28}$$

where $\theta = e_\varpi + \phi - \phi_d$.

The ABLFs V_v and V_ϖ are selected as follows:

$$\begin{aligned} V_v &= \frac{q_v}{2}\ln\frac{\lambda_v^2}{\lambda_v^2 - s_{1v}^2} + \frac{1-q_v}{2}\ln\frac{\lambda_v^2}{\lambda_v^2 - s_{1v}^2} \\ V_\varpi &= \frac{q_\varpi}{2}\ln\frac{\lambda_\varpi^2}{\lambda_\varpi^2 - s_{1\varpi}^2} + \frac{1-q_\varpi}{2}\ln\frac{\lambda_\varpi^2}{\lambda_\varpi^2 - s_{1\varpi}^2} \end{aligned} \tag{29}$$

where $\lambda_i (i = v, \omega)$ and $\bar{\lambda}_i (i = v, \omega)$ represent the designed parameters satisfying $\lambda_i l_i^{-1} \leq B_i$ and $\bar{\lambda}_i l_i^{-1} \leq B_i$, respectively. It should be noted that the inequalities $\lambda_v \leq s_{1v} \leq \bar{\lambda}_v$ and $\lambda_\omega \leq s_{1\omega} \leq \bar{\lambda}_\omega$ hold when V_v and V_ω are bounded, respectively.

By combining (26), (28), and (29), the derivatives of V_v and V_ω can be given by:

$$\dot{V}_v = \bar{s}_{1v} l_v \left(\dot{l}_v l_v^{-1} z_v - (s_{2v} + \alpha_v) \cos e_\omega + v_d \cos\theta \right) \tag{30}$$

$$\dot{V}_\omega = \bar{s}_{1\omega} l_\omega \left(\dot{l}_\omega l_\omega^{-1} z_\omega - (s_{2\omega} + \alpha_\omega) + \frac{v}{e_v} \sin e_\omega - \frac{v_d}{e_v} \sin\theta \right) \tag{31}$$

where $\bar{s}_{1v} = \frac{q_v s_{1v}}{\bar{\lambda}_v^2 - s_{1v}^2} + \frac{(1-q_v) s_{1v}}{\lambda_v^2 - s_{1v}^2}$ and $\bar{s}_{1\omega} = \frac{q_\omega s_{1v}}{\bar{\lambda}_\omega^2 - s_{1\omega}^2} + \frac{(1-q_\omega) s_{1v}}{\lambda_\omega^2 - s_{1\omega}^2}$, which are designed for simplifying the equations.

Then, construct the following virtual controllers:

$$\begin{aligned} \alpha_v = \frac{1}{\cos e_\omega} \Bigg[& \frac{f_v}{l_v} \left(\frac{k_{11v} q_v s_{1v}^3}{\bar{\lambda}_v^2 - s_{1v}^2} + \frac{k_{12v} q_v s_{1v}^{2\xi-1}}{\left(\bar{\lambda}_v^2 - s_{1v}^2\right)^{\xi-1}} + \frac{k_{21v}(1-q_v) s_{1v}^3}{\lambda_v^2 - s_{1v}^2} + \frac{k_{22v}(1-q_v) s_{1v}^{2\xi-1}}{\left(\lambda_v^2 - s_{1v}^2\right)^{\xi-1}} \right) \\ & + \dot{l}_v l_v^{-1} z_v + v_d \cos\theta \Bigg] \end{aligned} \tag{32}$$

$$\begin{aligned} \alpha_\omega = & \frac{f_\omega}{l_\omega} \left(\frac{k_{11\omega} q_\omega s_{1\omega}^3}{\bar{\lambda}_\omega^2 - s_{1\omega}^2} + \frac{k_{12\omega} q_\omega s_{1\omega}^{2\xi-1}}{\left(\bar{\lambda}_\omega^2 - s_{1\omega}^2\right)^{\xi-1}} + \frac{k_{21\omega}(1-q_\omega) s_{1\omega}^3}{\lambda_\omega^2 - s_{1\omega}^2} + \frac{k_{22\omega}(1-q_\omega) s_{1\omega}^{2\xi-1}}{\left(\lambda_\omega^2 - s_{1\omega}^2\right)^{\xi-1}} \right) \\ & + \dot{l}_\omega l_\omega^{-1} z_\omega + \frac{v}{e_v} \sin e_\omega - \frac{v_d}{e_v} \sin\theta \end{aligned} \tag{33}$$

where f_v and f_ω are positive-definite gain constants.

Remark 2. *According to Lemma 1, to ensure fixed-time convergence of the system, the value range of the designed parameter ξ is $(0, 1)$. However, ξ must also meet the following inequalities $2\xi - 1 > 0$ and $\xi - 1 < 0$ to prevent the singularity of the terms with ξ raised to the power, such as $\frac{k_{12v} q_v s_{1v}^{2\xi-1}}{\left(\bar{\lambda}_v^2 - s_{1v}^2\right)^{\xi-1}}$ and $\frac{k_{22v}(1-q_v) s_{1v}^{2\xi-1}}{\left(\lambda_v^2 - s_{1v}^2\right)^{\xi-1}}$. Therefore, the value of ξ must be selected in the range $\left(\frac{1}{2}, 1\right)$.*

By considering (32) and (33), new expressions of $\dot{V}_v$ and $\dot{V}_\omega$, respectively, can be obtained as follows:

$$\begin{aligned} \dot{V}_v = & -\frac{k_{11v} q_v f_v s_{1v}^4}{\left(\bar{\lambda}_v^2 - s_{1v}^2\right)^2} - \frac{k_{21v}(1-q_v) f_v s_{1v}^4}{\left(\lambda_v^2 - s_{1v}^2\right)^2} - \frac{k_{12v} q_v f_v s_{1v}^{2\xi}}{\left(\bar{\lambda}_v^2 - s_{1v}^2\right)^{\xi}} - \frac{k_{22v}(1-q_v) f_v s_{1v}^{2\xi}}{\left(\lambda_v^2 - s_{1v}^2\right)^{\xi}} \\ & - \bar{s}_{1v} l_v s_{2v} \cos e_\omega \end{aligned} \tag{34}$$

$$\begin{aligned} \dot{V}_\omega = & -\frac{k_{11\omega} q_\omega f_\omega s_{1\omega}^4}{\left(\bar{\lambda}_\omega^2 - s_{1\omega}^2\right)^2} - \frac{k_{21\omega}(1-q_\omega) f_\omega s_{1\omega}^4}{\left(\lambda_\omega^2 - s_{1\omega}^2\right)^2} - \frac{k_{12\omega} q_\omega f_\omega s_{1\omega}^{2\xi}}{\left(\bar{\lambda}_\omega^2 - s_{1\omega}^2\right)^{\xi}} - \frac{k_{22\omega}(1-q_\omega) f_\omega s_{1\omega}^{2\xi}}{\left(\lambda_\omega^2 - s_{1\omega}^2\right)^{\xi}} \\ & - \bar{s}_{1\omega} l_\omega s_{2\omega} \end{aligned} \tag{35}$$

Step 2. Aimed at conserving the information interchanging resources, the relative threshold ETM is introduced into the channel from the controller to the actuator. The event-triggered control law is designed as follows:

$$\begin{cases} \Omega_i(t) = -(1+\sigma_i) \left(\bar{u}_i \tanh\left(\frac{s_{2i} \bar{u}_i}{\vartheta_i} \right) + \bar{g}_i \tanh\left(\frac{s_{2i} \bar{g}_i}{\vartheta_i} \right) \right) \\ u_i(t) = \Omega_i(t_k), t_k \leq t < t_{k+1} \\ t_{k+1} = \inf\{ t \in R \,||\Delta_i(t)| \geq \sigma_i |u_i(t)| + g_i \} \end{cases} (i = v, \omega) \tag{36}$$

where $0 < \sigma_i < 1$, $\vartheta_i > 0$, $g_i > 0$, $\bar{g}_i > \frac{g_i}{1-\sigma_i}$; $\Delta_i(t) = \Omega_i(t_k) - u_i(t)$ represents the measurement error; $\bar{u}_i$ represents the intermediate control law, which would be designed

later; $t_k > 0$ denotes the triggering moment, and $k \in \mathbb{Z}^+$. The diagram that illustrates how ETM works in the control framework is shown in Figure 2.

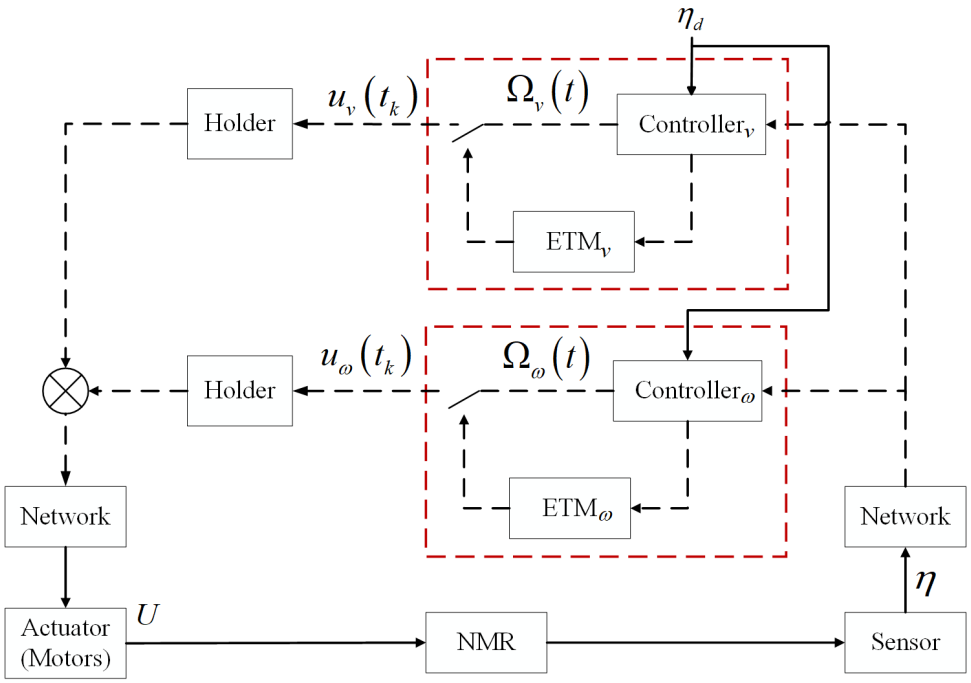

Figure 2. Diagram of the proposed control method.

Remark 3. *It can be surely acknowledged that it is more practical and beneficial to place the ETM in the sensor-to-controller channel, which could both help alleviate the communication burden and reduce computation cost. However, by utilizing the aforementioned method, it would render data discrete and lead to challenges for handling differential problems in the controller design process. Therefore, one focus spot of our future research would be to construct an ETM implemented in both sensor-to-controller and controller-to-actuator channels.*

From the first equation of (36) and the definition of $\Delta_i(t)$, the following inequality can be obtained:

$$u_i(t) = \frac{\Omega_i(t) - v_{2,i}(t)g_i}{1 + v_{1,i}(t)\sigma_i} \tag{37}$$

where $|v_{1,i}(t)| \leq 1$ and $|v_{2,i}(t)| \leq 1$.

According to Equations (36) and (37) and Lemma 2, it can be obtained as follows:

$$\begin{aligned} s_{2v}u_v(t) &\leq |s_{2v}\bar{u}_v| - s_{2v}\bar{u}_v \tanh\left(\frac{s_{2v}\bar{u}_v}{\vartheta_v}\right) - |s_{2v}\bar{u}_v| \\ &\quad + |s_{2v}\bar{g}_v| - s_{2v}\bar{g}_v \tanh\left(\frac{s_{2v}\bar{g}_v}{\vartheta_v}\right) \\ &\leq 0.557\vartheta_v + s_{2v}\bar{u}_v \end{aligned} \tag{38}$$

$$\begin{aligned} s_{2\omega}u_\omega(t) &\leq |s_{2\omega}\bar{u}_\omega| - s_{2\omega}\bar{u}_\omega \tanh\left(\frac{s_{2\omega}\bar{u}_\omega}{\vartheta_\omega}\right) - |s_{2\omega}\bar{u}_\omega| \\ &\quad + |s_{2\omega}\bar{g}_\omega| - s_{2\omega}\bar{g}_\omega \tanh\left(\frac{s_{2\omega}\bar{g}_\omega}{\vartheta_\omega}\right) \\ &\leq 0.557\vartheta_\omega + s_{2\omega}\bar{u}_\omega \end{aligned} \tag{39}$$

Then, by considering (3) and (26), it can be deduced that:

$$\frac{\dot{s}_{2v}}{m_v} = u_v + \Gamma_v^T \Phi_v \tag{40}$$

$$\frac{\dot{s}_{2\omega}}{m_\omega} = u_\omega + \Gamma_\omega^T \Phi_\omega \tag{41}$$

where $\Gamma_v = \left[\omega^2, -v, -\omega, -\dot{\alpha}_v\right]^T$ and $\Gamma_\omega = \left[-\omega v, -v, -\omega, -\dot{\alpha}_\omega\right]^T$. Both $\Phi_v = \left[\frac{2bc}{r}, \frac{d_1+d_2}{r}, \frac{b(d_1-d_2)}{r}, \frac{2(m_1+m_2)}{r}\right]^T$ and $\Phi_\omega = \left[\frac{2c}{r}, \frac{d_1-d_2}{r}, \frac{b(d_1+d_2)}{r}, \frac{2b(m_1-m_2)}{r}\right]^T$ are matrices with unknown parameters.

In this step, the ABLF is chosen as:

$$V = V_v + V_\omega + \frac{1}{2m_v} s_{2v}^2 + \frac{1}{2m_\omega} s_{2\omega}^2 + \frac{1}{2}\tilde{\Phi}_v^T \mathrm{K}_v^{-1} \tilde{\Phi}_v + \frac{1}{2}\tilde{\Phi}_\omega^T \mathrm{K}_\omega^{-1} \tilde{\Phi}_\omega \tag{42}$$

where $\tilde{\Phi}_i = \Phi_i - \hat{\Phi}_i \, (i = v, \omega)$ represents the error between the ideal unknown matrix Φ_i and its estimated value $\hat{\Phi}_i$; $\mathrm{K}_i^{-1} (i = v, \omega)$ denotes the inverse matrix of K_i, which is a 4×4 symmetric positive-definite gain matrix.

Differentiate Equation (42) by substituting from (38) to (41), we obtain:

$$\begin{aligned} \dot{V} \leq \dot{V}_v + \dot{V}_\omega + s_{2v}\left(\bar{u}_v + \Gamma_v^T \Phi_v\right) + s_{2\omega}\left(\bar{u}_\omega + \Gamma_\omega^T \Phi_\omega\right) - \tilde{\Phi}_v^T \mathrm{K}_v^{-1} \dot{\hat{\Phi}}_v - \tilde{\Phi}_\omega^T \mathrm{K}_\omega^{-1} \dot{\hat{\Phi}}_\omega \\ + 0.557\vartheta_v + 0.557\vartheta_\omega \end{aligned} \tag{43}$$

The parameter adaptive laws are defined as follows:

$$\dot{\hat{\Phi}}_v = \mathrm{K}_v \Gamma_v s_{2v} - \kappa_v \mathrm{K}_v \hat{\Phi}_v - h_v \mathrm{K}_v \hat{\Phi}_v^3 \tag{44}$$

$$\dot{\hat{\Phi}}_\omega = \mathrm{K}_\omega \Gamma_\omega s_{2\omega} - \kappa_\omega \mathrm{K}_\omega \hat{\Phi}_\omega - h_\omega \mathrm{K}_\omega \hat{\Phi}_\omega^3 \tag{45}$$

According to Lemma 3, it is true that:

$$\kappa_v \tilde{\Phi}_v^T \hat{\Phi}_v \leq -\frac{\kappa_v}{2}\tilde{\Phi}_v^T \tilde{\Phi}_v + \frac{\kappa_v}{2}\Phi_v^T \Phi_v \tag{46}$$

$$\kappa_\omega \tilde{\Phi}_\omega^T \hat{\Phi}_\omega \leq -\frac{\kappa_\omega}{2}\tilde{\Phi}_\omega^T \tilde{\Phi}_\omega + \frac{\kappa_\omega}{2}\Phi_\omega^T \Phi_\omega \tag{47}$$

From Lemma 4, by letting $\alpha = 1$, $\beta = \frac{\kappa_v}{2}\tilde{\Phi}_v^T \tilde{\Phi}_v$, $m_1 = 1 - \xi$, $m_2 = \xi$, $k = \xi^{\frac{\xi}{1-\xi}}$, one has:

$$\left(\frac{\kappa_v}{2}\tilde{\Phi}_v^T \tilde{\Phi}_v\right)^\xi \leq \iota + \frac{\kappa_v}{2}\tilde{\Phi}_v^T \tilde{\Phi}_v \tag{48}$$

where $\iota = (1 - \xi)\xi^{\frac{\xi}{1-\xi}}$.

In the similar way, the following inequality is obtained:

$$\left(\frac{\kappa_\omega}{2}\tilde{\Phi}_\omega^T \tilde{\Phi}_\omega\right)^\xi \leq \iota + \frac{\kappa_\omega}{2}\tilde{\Phi}_\omega^T \tilde{\Phi}_\omega \tag{49}$$

Substituting inequalities from (46) to (49) into (43), one has:

$$\begin{aligned} \dot{V} \leq \dot{V}_v + \dot{V}_\omega + s_{2v}\left(\bar{u}_v + \Gamma_v^T \Phi_v - \tilde{\Phi}_v^T \Gamma_v\right) + s_{2\omega}\left(\bar{u}_\omega + \Gamma_\omega^T \Phi_\omega - \tilde{\Phi}_\omega^T \Gamma_\omega\right) \\ - \frac{\kappa_v}{2}\tilde{\Phi}_v^T \tilde{\Phi}_v - \frac{\kappa_\omega}{2}\tilde{\Phi}_\omega^T \tilde{\Phi}_\omega + h_v \tilde{\Phi}_v^T \hat{\Phi}_v^3 + h_\omega \tilde{\Phi}_\omega^T \hat{\Phi}_\omega^3 + \Lambda_1 \end{aligned} \tag{50}$$

where $\Lambda_1 = \frac{\kappa_v}{2}\Phi_v^T \Phi_v + \frac{\kappa_\omega}{2}\Phi_\omega^T \Phi_\omega + 0.557\vartheta_v + 0.557\vartheta_\omega + 2\iota$.

Next, for the following equation:

$$h_v\tilde{\Phi}_{v,j}\hat{\Phi}_{v,j}^3 = h_v\tilde{\Phi}_{v,j}\left(\Phi_{v,j}^3 + 3\Phi_{v,j}\tilde{\Phi}_{v,j}^2 - 3\Phi_{v,j}^2\tilde{\Phi}_{v,j} - \tilde{\Phi}_{v,j}^3\right) \tag{51}$$

By utilizing Lemma 3, one has the following inequality:

$$\tilde{\Phi}_{v,j}\Phi_{v,j}^3 \leq \frac{\Phi_{v,j}^4}{12} + 3\Phi_{v,j}^2\tilde{\Phi}_{v,j}^2 \tag{52}$$

$$3\Phi_{v,j}^3\tilde{\Phi}_{v,j} \leq \frac{9\varsigma_{v,j}^{\frac{4}{3}}\tilde{\Phi}_{v,j}^4}{4} + \frac{3\Phi_{v,j}^4}{4\varsigma_{v,j}^4} \tag{53}$$

where $\varsigma_{v,j} > 0\,(j = 1, 2)$.

Substitute inequalities (52) and (53) into (51), one gets:

$$\begin{aligned} h_v\tilde{\Phi}_{v,j}\hat{\Phi}_{v,j}^3 &\leq -\left(4h_v - 9h_v\varsigma_{v,j}^{\frac{4}{3}}\right)\left(\frac{1}{2}\tilde{\Phi}_{v,j}^2\right)^2 + \frac{h_v\Phi_{v,j}^4}{12} + \frac{3h_v\Phi_{v,j}^4}{4\varsigma_{v,j}^4} \\ &\leq -\hbar_v\left(\frac{1}{2}\tilde{\Phi}_{v,j}^2\right)^2 + \frac{h_v\Phi_{v,j}^4}{12} + \frac{3h_v\Phi_{v,j}^4}{4\varsigma_{v,j}^4} \end{aligned} \tag{54}$$

where $\hbar_v = \min\left\{4 - 9\varsigma_{v,1}^{\frac{4}{3}}, 4 - 9\varsigma_{v,2}^{\frac{4}{3}}\right\}$.

Further, for $h_v\tilde{\Phi}_v^T\hat{\Phi}_v^3 = \sum_{j=1}^{2} h_{v,j}\tilde{\Phi}_{v,j}\hat{\Phi}_{v,j}^3$,

$$\begin{aligned} h_v\tilde{\Phi}_v^T\hat{\Phi}_v^3 &= \sum_{j=1}^{2} h_{v,j}\tilde{\Phi}_{v,j}\hat{\Phi}_{v,j}^3 \\ &\leq -\sum_{j=1}^{2}\hbar_v\left(\frac{1}{2}\tilde{\Phi}_{v,j}^2\right)^2 + \sum_{j=1}^{2}\frac{h_v\Phi_{v,j}^4}{12} + \sum_{j=1}^{2}\frac{3h_v\Phi_{v,j}^4}{4\varsigma_{v,j}^4} \\ &\leq -\bar{\hbar}_v\left(\frac{1}{2}\tilde{\Phi}_{v,j}^T K_{v,j}^{-1}\tilde{\Phi}_{v,j}\right)^2 + \sum_{j=1}^{2}\left(\frac{h_v\Phi_{v,j}^4}{12} + \frac{3h_v\Phi_{v,j}^4}{4\varsigma_{v,j}^4}\right) \end{aligned} \tag{55}$$

where $\bar{\hbar}_v = \frac{\hbar_v}{2\left(\lambda_{\max}\left(K_{v,j}^{-1}\right)\right)^2}$, $\lambda_{\max}\left(K_{v,j}^{-1}\right)$ is the maximum eigenvalue of $K_{v,j}^{-1}$. Similarly, we obtain:

$$\begin{aligned} h_\omega\tilde{\Phi}_\omega^T\hat{\Phi}_\omega^3 = \sum_{j=1}^{2} h_{\omega,j}\tilde{\Phi}_{\omega,j}\hat{\Phi}_{\omega,j}^3 &\leq -\sum_{j=1}^{2}\hbar_\omega\left(\frac{1}{2}\tilde{\Phi}_{\omega,j}^2\right)^2 + \sum_{j=1}^{2}\frac{h_\omega\Phi_{\omega,j}^4}{12} + \sum_{j=1}^{2}\frac{3h_\omega\Phi_{\omega,j}^4}{4\varsigma_{\omega,j}^4} \\ &\leq -\bar{\hbar}_\omega\left(\frac{1}{2}\tilde{\Phi}_{\omega,j}^T K_{\omega,j}^{-1}\tilde{\Phi}_{\omega,j}\right)^2 + \sum_{j=1}^{2}\left(\frac{h_\omega\Phi_{\omega,j}^4}{12} + \frac{3h_\omega\Phi_{\omega,j}^4}{4\varsigma_{\omega,j}^4}\right) \end{aligned} \tag{56}$$

where $\bar{\hbar}_\omega = \frac{\hbar_\omega}{2\left(\lambda_{\max}\left(K_{\omega,j}^{-1}\right)\right)^2}$, and $\lambda_{\max}\left(K_{\omega,j}^{-1}\right)$ is the maximum eigenvalue of $K_{\omega,j}^{-1}$.

By substituting inequalities (55) and (56) into (50), $\dot{V}$ can be written as:

$$\begin{aligned} \dot{V} \leq\ & s_{2v}\left(\bar{u}_v + \Gamma_v^T\hat{\Phi}_v\right) + s_{2\omega}\left(\bar{u}_\omega + \Gamma_\omega^T\hat{\Phi}_\omega\right) - \left(\frac{\kappa_v}{2}\tilde{\Phi}_v^T\tilde{\Phi}_v\right)^\xi - \left(\frac{\kappa_\omega}{2}\tilde{\Phi}_\omega^T\tilde{\Phi}_\omega\right)^\xi \\ & - \bar{\hbar}_v\left(\frac{1}{2}\tilde{\Phi}_{v,i}^T K_{v,i}^{-1}\tilde{\Phi}_{v,i}\right)^2 - \bar{\hbar}_{\omega,j}\left(\frac{1}{2}\tilde{\Phi}_{\omega,i}^T K_{\omega,i}^{-1}\tilde{\Phi}_{\omega,i}\right)^2 + \dot{V}_v + \dot{V}_\omega + \Lambda_2 \end{aligned} \tag{57}$$

where $\Lambda_2 = \Lambda_1 + \sum_{j=1}^{2}\left(\frac{h_v\Phi_{v,j}^4}{12} + \frac{3h_v\Phi_{v,j}^4}{4\varsigma_{v,j}^4}\right) + \sum_{j=1}^{2}\left(\frac{h_\omega\Phi_{\omega,j}^4}{12} + \frac{3h_\omega\Phi_{\omega,j}^4}{4\varsigma_{\omega,j}^4}\right)$.

Now, by inserting (34) and (35) into (57), one has:

$$\begin{aligned}\dot{V} \le & -\frac{k_{11v}q_v f_v s_{1v}^4}{\left(\lambda_v^2 - s_{1v}^2\right)^2} - \frac{k_{21v}(1-q_v) f_v s_{1v}^4}{\left(\lambda_v^2 - s_{1v}^2\right)^2} - \frac{k_{12v}q_v f_v s_{1v}^{2\xi}}{\left(\lambda_v^2 - s_{1v}^2\right)^\xi} - \frac{k_{22v}(1-q_v) f_v s_{1v}^{2\xi}}{\left(\lambda_v^2 - s_{1v}^2\right)^\xi} \\ & - \frac{k_{11\omega}q_\omega f_\omega s_{1\omega}^4}{\left(\lambda_\omega^2 - s_{1\omega}^2\right)^2} - \frac{k_{21\omega}(1-q_\omega) f_\omega s_{1\omega}^4}{\left(\lambda_\omega^2 - s_{1\omega}^2\right)^2} - \frac{k_{12\omega}q_\omega f_\omega s_{1\omega}^{2\xi}}{\left(\lambda_\omega^2 - s_{1\omega}^2\right)^\xi} - \frac{k_{22\omega}(1-q_\omega) f_\omega s_{1\omega}^{2\xi}}{\left(\lambda_\omega^2 - s_{1\omega}^2\right)^\xi} \\ & - \bar{s}_{1v} l_v s_{2v}\cos e_\omega - \bar{s}_{1\omega} l_\omega s_{2\omega} + s_{2v}\left(\bar{u}_v + \Gamma_v^T\hat{\Phi}_v\right) + s_{2\omega}\left(\bar{u}_\omega + \Gamma_\omega^T\hat{\Phi}_\omega\right) \\ & - \left(\frac{\kappa_v}{2}\tilde{\Phi}_v^T\tilde{\Phi}_v\right)^\xi - \left(\frac{\kappa_\omega}{2}\tilde{\Phi}_\omega^T\tilde{\Phi}_\omega\right)^\xi - \bar{\hbar}_v\left(\frac{1}{2}\tilde{\Phi}_{v,i}^T K_{v,i}^{-1}\tilde{\Phi}_{v,i}\right)^2 - \bar{\hbar}_\omega\left(\frac{1}{2}\tilde{\Phi}_{\omega,i}^T K_{\omega,i}^{-1}\tilde{\Phi}_{\omega,i}\right)^2 + \Lambda_2\end{aligned} \tag{58}$$

Subsequently, the intermediate control laws are constructed as follows:

$$\bar{u}_v = -\eta_{v,1}s_{2v}^3 - \eta_{v,2}s_{2v}^{2\xi-1} - \Gamma_v^T\hat{\Phi}_v + \bar{s}_{1v}l_v\cos e_\omega \tag{59}$$

$$\bar{u}_\omega = -\eta_{\omega,1}s_{2\omega}^3 - \eta_{\omega,2}s_{2\omega}^{2\xi-1} - \Gamma_\omega^T\hat{\Phi}_\omega + \bar{s}_{1\omega}l_\omega \tag{60}$$

$$\bar{u}_v = u_1 + u_2, \bar{u}_\omega = u_1 - u_2 \tag{61}$$

Obviously, it can be deduced that:

$$\begin{aligned}\dot{V} \le & -4k_{11v}f_v\left(\frac{q_v s_{1v}^2}{2\left(\lambda_v^2 - s_{1v}^2\right)}\right)^2 - 4k_{21v}f_v\left(\frac{(1-q_v)s_{1v}^2}{2\left(\lambda_v^2 - s_{1v}^2\right)}\right)^2 - 2^\xi k_{12v}f_v\left(\frac{q_v s_{1v}^2}{2\left(\lambda_v^2 - s_{1v}^2\right)}\right)^\xi - 2^\xi k_{22v}f_v\left(\frac{(1-q_v)s_{1v}^2}{2\left(\lambda_v^2 - s_{1v}^2\right)}\right)^\xi \\ & - 4k_{11\omega}f_\omega\left(\frac{q_\omega s_{1\omega}^2}{2\left(\lambda_\omega^2 - s_{1\omega}^2\right)}\right)^2 - 4k_{21\omega}f_\omega\left(\frac{(1-q_\omega)s_{1\omega}^2}{2\left(\lambda_\omega^2 - s_{1\omega}^2\right)}\right)^2 - 2^\xi k_{12\omega}f_\omega\left(\frac{q_\omega s_{1\omega}^2}{2\left(\lambda_\omega^2 - s_{1\omega}^2\right)}\right)^\xi - 2^\xi k_{22\omega}f_\omega\left(\frac{(1-q_\omega)s_{1\omega}^2}{2\left(\lambda_\omega^2 - s_{1\omega}^2\right)}\right)^\xi \\ & - 4m_v^2\eta_{v,1}\left(\frac{1}{2m_v}s_{2v}^2\right)^2 - 2^\xi m_v^\xi\eta_{v,2}\left(\frac{1}{2m_v}s_{2v}^2\right)^\xi - 4m_\omega^2\eta_{\omega,1}\left(\frac{1}{2m_\omega}s_{2\omega}^2\right)^2 - 2^\xi m_\omega^\xi\eta_{\omega,2}\left(\frac{1}{2m_\omega}s_{2\omega}^2\right)^\xi \\ & - \left(\frac{\kappa_v}{\lambda_{\max}\left(K_{v,i}^{-1}\right)}\right)^\xi\left(\frac{1}{2}\tilde{\Phi}_v^T K_{v,i}^{-1}\tilde{\Phi}_v\right)^\xi - \left(\frac{\kappa_\omega}{\lambda_{\max}\left(K_{\omega,i}^{-1}\right)}\right)^\xi\left(\frac{1}{2}\tilde{\Phi}_\omega^T K_{\omega,i}^{-1}\tilde{\Phi}_\omega\right)^\xi - \bar{\hbar}_v\left(\frac{1}{2}\tilde{\Phi}_{v,i}^T K_{v,i}^{-1}\tilde{\Phi}_{v,i}\right)^2 - \bar{\hbar}_\omega\left(\frac{1}{2}\tilde{\Phi}_{\omega,i}^T K_{\omega,i}^{-1}\tilde{\Phi}_{\omega,i}\right)^2 \\ & + \Lambda_2\end{aligned} \tag{62}$$

For convenience, it can be rewritten as:

$$\begin{aligned}\dot{V} \le & -\gamma_{1v,1}\left(\frac{q_v s_{1v}^2}{2\left(\lambda_v^2 - s_{1v}^2\right)}\right)^2 - \gamma_{1v,j,2}\left(\frac{(1-q_v)s_{1v}^2}{2\left(\lambda_v^2 - s_{1v}^2\right)}\right)^2 - \gamma_{1\omega,1}\left(\frac{q_\omega s_{1\omega}^2}{2\left(\lambda_\omega^2 - s_{1\omega}^2\right)}\right)^2 - \gamma_{1\omega,2}\left(\frac{(1-q_\omega)s_{1\omega}^2}{2\left(\lambda_\omega^2 - s_{1\omega}^2\right)}\right)^2 \\ & - \gamma_{1v,3}\left(\frac{1}{2m_v}s_{2v}^2\right)^2 - \gamma_{1\omega,3}\left(\frac{1}{2m_\omega}s_{2\omega}^2\right)^2 - \bar{\hbar}_v\left(\frac{1}{2}\tilde{\Phi}_{v,j}^T K_{v,j}^{-1}\tilde{\Phi}_{v,j}\right)^2 - \bar{\hbar}_\omega\left(\frac{1}{2}\tilde{\Phi}_{\omega,j}^T K_{\omega,j}^{-1}\tilde{\Phi}_{\omega,j}\right)^2 \\ & - \gamma_{2v,1}\left(\frac{q_v s_{1v}^2}{2\left(\lambda_v^2 - s_{1v}^2\right)}\right)^\xi - \gamma_{2v,2}\left(\frac{(1-q_v)s_{1v}^2}{2\left(\lambda_v^2 - s_{1v}^2\right)}\right)^\xi - \gamma_{2\omega,1}\left(\frac{q_\omega s_{1\omega}^2}{2\left(\lambda_\omega^2 - s_{1\omega}^2\right)}\right)^\xi - \gamma_{2\omega,2}\left(\frac{(1-q_\omega)s_{1\omega}^2}{2\left(\lambda_\omega^2 - s_{1\omega}^2\right)}\right)^\xi \\ & - \gamma_{2v,3}\left(\frac{1}{2m_v}s_{2v}^2\right)^\xi - \gamma_{2\omega,3}\left(\frac{1}{2m_\omega}s_{2\omega}^2\right)^\xi - \gamma_{2v,4}\left(\frac{1}{2}\tilde{\Phi}_v^T K_{v,j}^{-1}\tilde{\Phi}_v\right)^\xi - \gamma_{2\omega,4}\left(\frac{1}{2}\tilde{\Phi}_\omega^T K_{\omega,j}^{-1}\tilde{\Phi}_\omega\right)^\xi + \Lambda_2\end{aligned} \tag{63}$$

where $\gamma_{1v,1} = 4k_{11v}f_v$, $\gamma_{1v,2} = 4k_{21v}f_v$, $\gamma_{1v,3} = 4m_v^2\eta_{v,1}$, $\gamma_{1\omega,1} = 4k_{11\omega}f_\omega$, $\gamma_{1\omega,2} = 4k_{21\omega}f_\omega$, $\gamma_{1\omega,3} = 4m_\omega^2\eta_{\omega,1}$, $\gamma_{2v,1} = 2^\xi k_{12v}f_v$, $\gamma_{2v,2} = 2^\xi k_{22v}f_v$, $\gamma_{2v,3} = 2^\xi m_v^\xi\eta_{v,2}$, $\gamma_{2v,4} = \left(\frac{\kappa_v}{\lambda_{\max}\left(K_{v,j}^{-1}\right)}\right)^\xi$, $\gamma_{2\omega,1} = 2^\xi k_{12\omega}f_\omega$, $\gamma_{2\omega,2} = 2^\xi k_{22\omega}f_\omega$, $\gamma_{2\omega,3} = 2^\xi m_\omega^\xi\eta_{\omega,2}$, $\gamma_{2\omega,4} = \left(\frac{\kappa_\omega}{\lambda_{\max}\left(K_{\omega,j}^{-1}\right)}\right)^\xi$, and $\bar{\hbar}_v, \bar{\hbar}_\omega$; Λ_2 was defined before.

Based on (63) and Lemma 5, it holds that:

$$\dot{V} \le -\gamma_1 V^2 - \gamma_2 V^\xi + \Lambda_2 \tag{64}$$

where $\gamma_1 = \frac{\min\{\gamma_{1v,1},\gamma_{1v,2},\gamma_{1v,3},\gamma_{1\omega,1},\gamma_{1\omega,2},\gamma_{1\omega,3},\bar{h}_v,\bar{h}_\omega\}}{8}$, $\gamma_2 = \min\{\gamma_{2v,1},\gamma_{2v,2},\gamma_{2v,3},\gamma_{2v,4},\gamma_{2\omega,1},\gamma_{2\omega,2},\gamma_{2\omega,3},\gamma_{2\omega,4}\}$, $\Lambda_2 = \frac{\kappa_v}{2}\Phi_v^T\Phi_v + \frac{\kappa_\omega}{2}\Phi_\omega^T\Phi_\omega + 0.557\vartheta_v + 0.557\vartheta_\omega + 2\iota + \sum_{j=1}^{2}\left(\frac{h_v\Phi_{v,j}^4}{12} + \frac{3h_v\Phi_{v,j}^4}{4\varsigma_{v,j}^4}\right) + \sum_{j=1}^{2}\left(\frac{h_\omega\Phi_{\omega,j}^4}{12} + \frac{3h_\omega\Phi_{\omega,j}^4}{4\varsigma_{\omega,j}^4}\right)$.

3.2. Stability Analysis

Theorem 1. *Consider the NMR system* (1)*; by constructing virtual controllers* (32), (33) *and using parameter adaptive law* (44), (45)*, intermediate control law* (59)–(61)*, and ETM* (36)*, it can be achieved that:*

(1) All the signals are bounded, and the tracking error system (11) *converges to prescribed regions* $\{z_v|-\lambda_v Q^{-1} \le z_v \le \lambda_v Q^{-1}\}$ *and* $\{z_\omega|-\lambda_\omega Q^{-1} \le z_\omega \le \lambda_\omega Q^{-1}\}$ *within a bounded settling time of the system.*

(2) Zeno phenomenon will not present.

Proof of Theorem 1 (1). From Lemma 1 and Equation (64), it can be concluded that the convergence time of the system (1) is practical fixed-time, and satisfies:

$$T \le \frac{1}{\gamma_1\Theta} + \frac{1}{\gamma_2\Theta(1-\xi)} \tag{65}$$

where $0 < \Theta < 1$.

Furthermore, it can be obtained that the trajectories of transformation errors s_{1v} and $s_{1\omega}$ satisfy:

$$\delta = \left\{ s_{1i}|V \le \min\left\{\left(\frac{\Lambda}{(1-\Theta)\gamma_1}\right)^{\frac{1}{2}}, \left(\frac{\Lambda}{(1-\Theta)\gamma_2}\right)^{\frac{1}{\xi}}\right\}\right\}(i = v, \omega) \tag{66}$$

From (29) and (42), the ABLFs are chosen as:

$$V_v = \frac{q_v}{2}\ln\frac{\lambda_v^2}{\lambda_v^2 - s_{1v}^2} + \frac{1-q_v}{2}\ln\frac{\lambda_v^2}{\lambda_v^2 - s_{1v}^2} \tag{67}$$

$$V_\omega = \frac{q_\omega}{2}\ln\frac{\lambda_\omega^2}{\lambda_\omega^2 - s_{1\omega}^2} + \frac{1-q_\omega}{2}\ln\frac{\lambda_\omega^2}{\lambda_\omega^2 - s_{1\omega}^2} \tag{68}$$

$$V = V_v + V_\omega + \frac{1}{2m_v}s_{2v}^2 + \frac{1}{2m_\omega}s_{2\omega}^2 + \frac{1}{2}\tilde{\Phi}_v^T\mathrm{K}_v^{-1}\tilde{\Phi}_v + \frac{1}{2}\tilde{\Phi}_\omega^T\mathrm{K}_\omega^{-1}\tilde{\Phi}_\omega \tag{69}$$

It can be obviously deduced that the last four items on the right side of function V are entirely semi-positive. Combining from (66) to (68), the following inequalities hold:

$$\begin{cases} V_v \le V_v + V_\omega \le V \\ V_\omega \le V_v + V_\omega \le V \end{cases} \tag{70}$$

$$\frac{q_v}{2}\ln\frac{\lambda_v^2}{\lambda_v^2 - s_{1v}^2} + \frac{1-q_v}{2}\ln\frac{\lambda_v^2}{\lambda_v^2 - s_{1v}^2} \le V \le \delta \tag{71}$$

$$\frac{q_\omega}{2}\ln\frac{\lambda_\omega^2}{\lambda_\omega^2 - s_{1\omega}^2} + \frac{1-q_\omega}{2}\ln\frac{\lambda_\omega^2}{\lambda_\omega^2 - s_{1\omega}^2} \le V \le \delta \tag{72}$$

Case 1. If $q_i = 1$, (71) and (72) can be simplified as follows:

$$\frac{1}{2}\ln\frac{\lambda_v^2}{\lambda_v^2 - s_{1v}^2} \le \delta \tag{73}$$

$$\frac{1}{2}\ln\frac{\lambda_{\omega}^{2}}{\lambda_{\omega}^{2}-s_{1\omega}^{2}}\leq\delta \tag{74}$$

According to the relationship between e^{x} and lnx, we can obtain that $e^{\ln x}=x$. Thus, the following equations can be deduced.

$$\frac{\lambda_{v}^{2}}{\lambda_{v}^{2}-s_{1v}^{2}}\leq e^{2\delta} \tag{75}$$

$$\frac{\lambda_{\omega}^{2}}{\lambda_{\omega}^{2}-s_{1\omega}^{2}}\leq e^{2\delta} \tag{76}$$

It is known that $\sqrt{1-e^{-\rho_i}}<1(\rho_i=2\delta>0)$ holds. Therefore, by a simplification operation, it can be obtained as follows:

$$s_{1v}\leq\lambda_{v}\sqrt{1-e^{-\rho_{v}}}<\lambda_{v} \tag{77}$$

$$s_{1\omega}\leq\lambda_{\omega}\sqrt{1-e^{-\rho_{\omega}}}<\lambda_{\omega} \tag{78}$$

Case 2. If $q_i=0$, it is similar to the deduction in Case 1. However, it is worth mentioning that, here, s_{1i} becomes negative. Thus, the consequence in Case 2 is presented as follows:

$$-\lambda_{v}\leq-\lambda_{v}\sqrt{1-e^{-\rho_{v}}}\leq s_{1v} \tag{79}$$

$$-\lambda_{\omega}\leq-\lambda_{\omega}\sqrt{1-e^{-\rho_{\omega}}}\leq s_{1\omega} \tag{80}$$

By further deduction, it yields:

$$-\lambda_{v}\leq-\lambda_{v}\sqrt{1-e^{-\rho_{v}}}\leq s_{1v}\leq\lambda_{v}\sqrt{1-e^{-\rho_{v}}}<\lambda_{v} \tag{81}$$

$$-\lambda_{\omega}\leq-\lambda_{\omega}\sqrt{1-e^{-\rho_{\omega}}}\leq s_{1\omega}\leq\lambda_{\omega}\sqrt{1-e^{-\rho_{\omega}}}<\lambda_{\omega} \tag{82}$$

where $\rho_v=\rho_\omega=2\delta>0$.

Thus, combining with (16), the following inequalities can be obtained:

$$-B_{1v}\leq-\frac{\lambda_{v}}{l_{v}}\leq z_{v}\leq\frac{\lambda_{v}}{l_{v}}\leq B_{2v} \tag{83}$$

$$-B_{1\omega}\leq-\frac{\lambda_{\omega}}{l_{\omega}}\leq z_{\omega}\leq\frac{\lambda_{\omega}}{l_{\omega}}\leq B_{2\omega} \tag{84}$$

According to the definition of V, we can obtain that all the errors s_{1v}, s_{2v}, $s_{1\omega}$, $s_{2\omega}$, $\tilde{\Phi}_v$, and $\tilde{\Phi}_\omega$ are bounded. As $\tilde{\Phi}_v$ and Φ_v are bounded variables, then $\tilde{\Phi}_v=\Phi_v-\hat{\Phi}_v$, and one can obtain that $\hat{\Phi}_v$ is bounded. In the same way, we can get that $\hat{\Phi}_\omega$ is also bounded. Additionally, according to the definition of α_v and α_ω, it can be deduced that α_v and α_ω are bounded. Last but not least, the boundness of u_v, u_ω, $\bar{u}_v$, and $\bar{u}_\omega$ are yielded from (36), (59), (60), and (61).

Ultimately, by utilizing the proposed method, it can be proved that all the signals are bounded, and the tracking error system (11) converges to prescribed regions $\left\{z_v|-\lambda_vQ^{-1}\leq z_v\leq\lambda_vQ^{-1}\right\}$ and $\left\{z_\omega\,|-\lambda_\omega Q^{-1}\leq z_\omega\leq\lambda_\omega Q^{-1}\right\}$ within a bounded settling time of the system. □

Proof of Theorem 1 (2). According to (36), the derivative of $\Delta_i(t)$ satisfies the following inequality:

$$\frac{d}{dt}|\Delta_{i}(t)|\leq\left|\dot{\Omega}_{i}(t)\right|\leq\widehat{\Omega}_{i} \tag{85}$$

where $\widehat{\Omega}_i$ represents the upper boundary of $\left|\dot{\Omega}_i(t)\right|$.

As $\lim_{t_k \to t_{k+1}} \Delta_i(t) \geq \Omega_i(t) - u_i$ and $\Delta_i(t_k) = 0$, the following inequality can be obtained:

$$\lim_{t_k \to t_{k+1}} \frac{d}{dt}|\Delta_i(t)| \geq \frac{\sigma_i|u_i| + g_i}{t_{k+1} - t_k} \geq \frac{g_i}{t_{k+1} - t_k} \tag{86}$$

Further, it can be seen that:

$$0 < \frac{g_i}{\widehat{\Omega}_i} \leq t_{k+1} - t_k \tag{87}$$

That is, it can be deduced that there exists the minimal interval triggered time $\frac{g_i}{\widehat{\Omega}_i}$ between any two continuous triggering to prevent Zeno behavior from happening. Furthermore, increasing the value of the specified parameter g_i could help extend the minimal interval triggered time. Additionally, the more the value of the designed parameter σ_i increases, the more communication resources could be reserved. □

At this point, the proof process is completed.

The proposed theorem has been proved. With the proposed adaptive event-triggered tracking control method, it can be deduced that the NMR system, which has asymmetric relative distance and bearing angle constraints, is capable of converging with guaranteed performance within a bounded settling time of the system.

Remark 4. *On the foundation of the aforementioned analysis, it can be deduced that the upper bound of convergence time of the system can be defined, which is independent of different system's initial conditions. Furthermore, it can be also obtained that by choosing different values of* ξ, γ_1, γ_2, *and* Θ, *different upper bounds of the convergence time can be selected. Then,* γ_1 *and* γ_2 *can be defined by the designed parameters such as* $\gamma_{1v,1}$, $\gamma_{1v,2}$, $\gamma_{1v,3}$, $\gamma_{1\omega,1}$, $\gamma_{1\omega,2}$, $\gamma_{1\omega,3}$, $\bar{\bar{h}}_v$, $\bar{\bar{h}}_\omega$, $\gamma_{2v,1}$, $\gamma_{2v,2}$, $\gamma_{2v,3}$, $\gamma_{2v,4}$, *and* $\gamma_{2\omega,1}$.

4. Simulations

In this section, aimed at verifying the validity of the proposed adaptive tracking control strategy, two practical simulation examples under different trajectories are considered. The values of system parameters are given in Table 1. Referred from [34], the inertia matrix parameters are given by the following equations:

$$\begin{aligned} m_1 &= \frac{1}{4}b^{-2}r^2\left(m_e b^2 + I\right) \\ m_2 &= \frac{1}{4}b^{-2}r^2\left(m_e b^2 - I\right) \\ m_e &= m_b + 2m_w \\ I &= m_b a^2 + 2m_w b^2 + I_b + 2I_m \end{aligned} \tag{88}$$

where m_1 and m_2 represent the masses of a robot body and a single propelling wheel equipped with a motor, respectively; a denotes the distance between the center of robot mass P_c and the center of wheel axis P_w. In addition, I_b, I_w, and I_m are the robot body's moment of inertia about the vertical axis through P_c, one propelling wheel's moment of inertia about the wheel axis P_w, and one propelling wheel's moment of inertia about the wheel diameter, respectively.

The Coriolis coefficient can be obtained as follows:

$$c = \frac{1}{2}b^{-1}r^2 m_b a \tag{89}$$

The simulation objective is to enable the NMR to dislodge the enemy under a desired trajectory given by (4), and the relative distance and bearing angle constraints would never be violated. That is, the robot can always keep a safety distance from the enemy to avoid

collision and maintain the enemy's visibility by the cameras and sensors equipped on the robot.

According to Equation (4), a series of various trajectories can be generated by appointing different values for v_d and ϖ_d, involving a static point, a straight line with different length, a circle with a radius of $\frac{v_d}{\varpi_d}$, etc.

Table 1. NMRs parameters (data from [34]).

Variable	Value	Variable	Value
b	0.75 [m]	I_b	15.625 [kg·m^2]
a	0.30 [m]	I_w	0.0050 [kg·m^2]
r	0.15 [m]	I_m	0.0025 [kg·m^2]
m_b	30 [kg]	d_1	5 [kg·m^2·s^{-1}]
m_w	1 [kg]	d_2	5 [kg·m^2·s^{-1}]

4.1. Example 1: Circle Trajectory

To generate the desired circle dislodging trajectory with a radius of 20 m, the following parameters are considered:

$$\begin{cases} x_d = 20\sin(0.1t) \\ y_d = 20\,(1-\cos(0.1t)) \\ \phi_d = 0.1t \\ v_d = 2 \\ \varpi_d = 0.1 \end{cases} \tag{90}$$

The system's initial conditions are presented as Cases I, II, and III in Table 2. The parameters of relative posture are given in the first line of Table 3. The designed parameters are shown in the second line of Table 3. It is worth pointing out that the relative distance and bearing angle constraints consisting of (8)–(10) would never be violated when Equations (12) and (13) hold. Thus, the parameters of PPF are selected in the third line of Table 3 for better convergence property of the tracking error system (11). In addition, the parameters related to ETM are given in the last line of Table 3.

Table 2. NMR initial conditions in Example 1.

Case	$x(0)$	$y(0)$	$\phi(0)$	$v(0)$	$\varpi(0)$
I	-0.2 [m]	0.8 [m]	$-\frac{\pi}{4}$ [rad]	1 [m/s]	0 [rad/s]
II	-1.4 [m]	-0.6 [m]	$-\frac{\pi}{6}$ [rad]	3 [m/s]	0.8 [rad/s]
III	-1.6 [m]	0.2 [m]	0 [rad]	1.8 [m/s]	2.4 [rad/s]

The simulation results are presented in Figure 3. According to Figure 3, the proposed tracking control scheme is instrumental for a type of NMR with asymmetric relative distance and bearing angle constraints. Figure 3a displays the enemy's reference trajectory and real trajectory (robot's output trajectory), which show an ideal performance that the robot can effectively dislodge the target under a certain trajectory. Figure 3b,c show the tracking error of relative distance and bearing angle, respectively. It is obvious that all the tracking errors converge into a predefined region given by PPF in a short time and never break away from the bounded area. Next, the curve of control torque input applied about the linear and angular axis are depicted in Figure 3d,e, respectively. It is worth pointing out that the blue curve represents the system's original input and the red one is the input under the event-triggered mechanism (ETM). Accordingly, we can obtain that the control torque inputs are bounded. The triggered time intervals are given in Figure 3f, which depicts that the maximal triggered time intervals of $u_v(t)$ and $u_\varpi(t)$ are 0.15 s and

0.14 s, respectively. Figure 3g and Table 4 reveal that the ETM reduces the triggered number to conserve communication resources, as the total triggered numbers based on the time-triggered mechanism (TTM) and ETM are 12,000 and 2591, respectively. That is, 78.408% of communication resources are successfully conserved by introducing ETM into the channel from the controller to the actuator. In Figure 3h,i, the estimated values of Φ_v and Φ_ω, respectively, are given and successfully verify that $\hat{\Phi}_v$ and $\hat{\Phi}_v$ are bounded parameters.

Table 3. The specified parameters and the controller parameters of Example 1.

The parameters of relative posture	$E_{1v} = 1.2\,[\mathrm{m}]$, $E_{2v} = 0.95\,[\mathrm{m}]$, $E_{1\omega} = 0.1\,[\mathrm{rad}]$, $E_{2\omega} = -0.05\,[\mathrm{rad}]$, $\bar{E}_v = 1\,[\mathrm{m}]$, $\bar{E}_\omega = 0\,[\mathrm{rad}]$.
The parameters of controllers	$\xi = 74/101$, $k_{11v} = k_{21v} = 34$, $k_{12v} = k_{22v} = 3$, $k_{11\omega} = k_{21\omega} = 28$, $k_{12\omega} = k_{22\omega} = 2$, $f_v = 2$, $f_\omega = 4$, $\eta_{v,1} = \eta_{v,2} = 2.2$, $\eta_{\omega,1} = \eta_{\omega,2} = 1.3$, $\kappa_v = h_v = 0.2$, $\kappa_\omega = h_\omega = 0.3$, $\mathrm{K}_v = diag(0.1, 0.1, 0.1, 0.01)$, $\mathrm{K}_\omega = diag(0.1, 0.1, 0.1, 0.02)$, $\hat{\Phi}_v(0) = \hat{\Phi}_\omega(0) = [0,0,0,0]^T$.
The parameters of PPF	$B_{1v} = (1-0.2)e^{-0.25t} + 0.2$, $B_{2v} = (1-0.05)e^{-0.25t} + 0.05$, $B_{1\omega} = (1-0.1)e^{-0.25t} + 0.1$, $B_{2\omega} = (1-0.05)e^{-0.25t} + 0.05$, $\chi_v = \chi_\omega = 4$, $Q_v = Q_\omega = 20$, $\lambda_v = 4$, $\lambda_v = 1$,$\lambda_\omega = 2$, $\lambda_\omega = 1$.
The parameter of ETM	$\vartheta_v = 5$, $\vartheta_\omega = 2.6$, $\sigma_v = 0.006$, $\sigma_\omega = 0.001$, $g_v = 0.01$, $g_\omega = 0.001$.

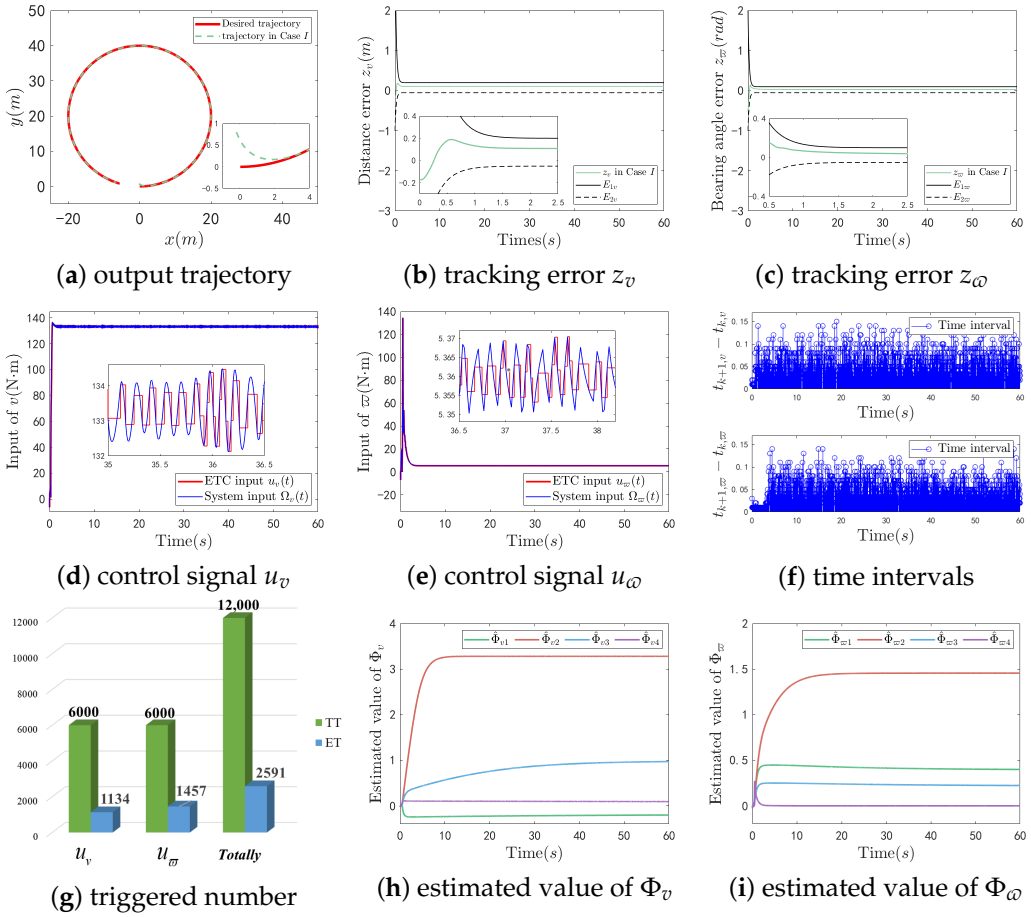

(**a**) output trajectory (**b**) tracking error z_v (**c**) tracking error z_ω

(**d**) control signal u_v (**e**) control signal u_ω (**f**) time intervals

(**g**) triggered number (**h**) estimated value of Φ_v (**i**) estimated value of Φ_ω

Figure 3. The simulation results of Example 1 in Case *I*.

On the basis of the above simulation results of Figure 3 and Table 4, it can be seen that the NMR system achieves the ideal performance using the proposed adaptive tracking control strategy. The system effectively conserves the communication resources while no Zeno behavior presents. Furthermore, the tracking errors can quickly converge to the predefined area with guaranteed transient and steady performance under relative distance and bearing angle constraints, even in different initial states of the system.

In addition, it can be perceived from Figure 4 that the convergence time of relative distance error and bearing angle error under different initial conditions can always be held around 0.52 s and 0.66 s, respectively, meaning that the range of the system's convergence time is not impacted by different initial conditions of the system.

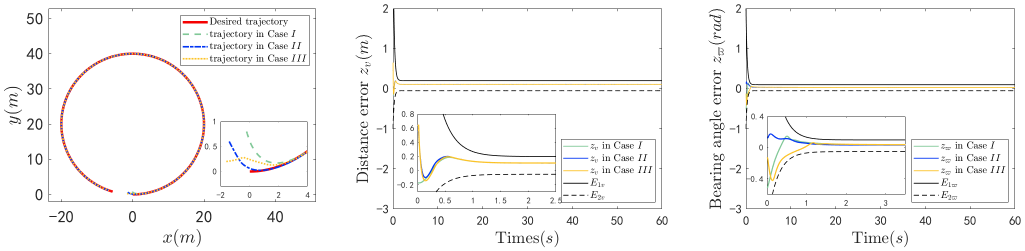

(**a**) output trajectory (**b**) tracking error z_v (**c**) tracking error z_ϖ

Figure 4. The tracking effect comparison of Example 1 among Cases *I*, *II*, and *III*.

Table 4. Triggered number of Example I in Case *I*.

Triggered Number / **Object** / **Scheme**	u_v	u_ϖ	**Total**
Time-Triggered Scheme	6000	6000	12,000
Event-Triggered Scheme	1134	1457	2591
The Rate	81.100%	75.717%	78.408%

Take ETM implemented on u_ϖ as an example. Aimed at comparing the ETM effect on different values of parameters, five sets of values are selected to complement the comparison. For convenience, the basic parameters are selected as Example I in Case *I*. In addition, we take $\sigma_v = \sigma_\varpi = \sigma_i (i = v, \varpi)$, and $g_v = g_\varpi = g_i (i = v, \varpi)$. The results are as shown in Figure 5.

Considering the triggered threshold of the ETM, it can be seen that the variables σ_i and g_i show positive correlation with the threshold. That is, by increasing σ_i or g_i, the triggered threshold would be increased, then the triggered number would be reduced and the triggered intervals would be longer. Simultaneously, it can be deduced that a smaller threshold could have more precise control applied to the system, then better system performance can be obtained. Referring to the above regulation, which is shown in Figure 5, we can choose appropriate triggered parameters to balance system performance and communication resources occupation.

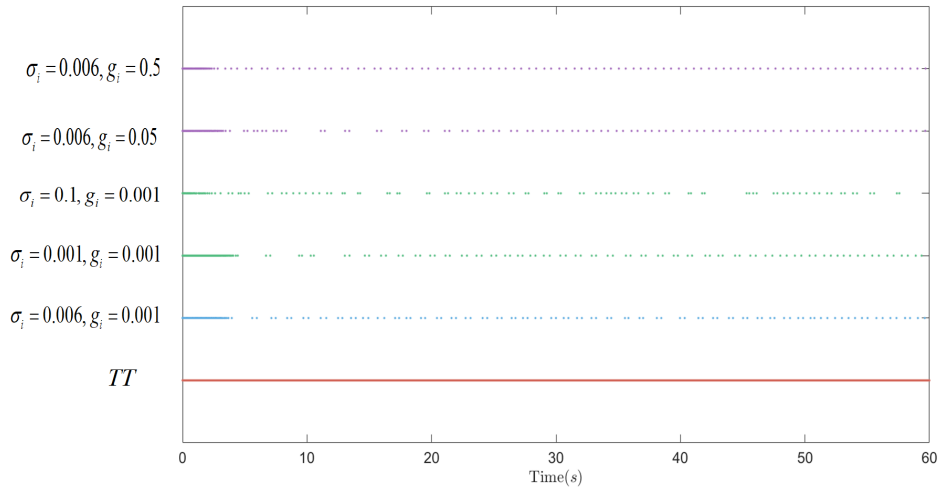

Figure 5. Illustration of triggered number by selecting different values of σ_i and g_i in comparison with time-triggered mechanism (TT).

4.2. Example 2: Varied Radius Trajectory

To further describe the validation of the proposed method, the desired dislodging trajectory is divided into two sections in this simulation experiment. For the first section, the trajectory is a semicircle with a radius of 24 m, which would last from 0 s to 15.7 s, and its parameters are selected as follows:

$$\begin{cases} x_d = 24\sin(0.2t) \\ y_d = 24\cos(0.2t + \pi) \\ \phi_d = 0.2t \\ v_d = 4.8 \\ \omega_d = 0.2 \end{cases} \tag{91}$$

For the second section, the trajectory is a circular arc with a radius of 32 m, which would last from 15.7 s to 50 s, and its parameters are chosen as follows:

$$\begin{cases} x_d = 32\sin(0.15t + 0.25\pi) \\ y_d = 32\cos(0.15t + 1.25\pi) - 8 \\ \phi_d = 0.15(t - 5\pi) \\ v_d = 4.8 \\ \omega_d = 0.15 \end{cases} \tag{92}$$

The system's initial conditions are presented as Cases I, II, and III in Table 5. Similar to Example 1, the parameters of relative posture, the parameters of controllers, the parameters of PPF, and the parameters of ETM are presented in Table 6. In addition, the tracking effect comparison among Cases I, II, and III is given in Figure 6.

As shown in Figures 6a and 7a, the robots are capable of convergence to the desired trajectory. Figures 6b,c and 7b,c depict that the relative distance error and bearing angle error could rapidly converge into a specified asymmetric region within 1 s and 0.8 s, respectively. In Figure 7d,e, it is shown that the ETM makes great contributions for the input signals to ease the burden of communication channels. Statistically, from Figure 7f,g and Table 7, at least 63.020% of communication resources can be preserved. Figure 7h,i depict that the estimated values of both Φ_v and Φ_ω are bounded. From the aforementioned analysis, it is obvious that the results of Example 2 are quite similar to Example 1. That is, the proposed control scheme can practically guarantee the system performance while the system achieves fixed-time convergence under asymmetric constraints.

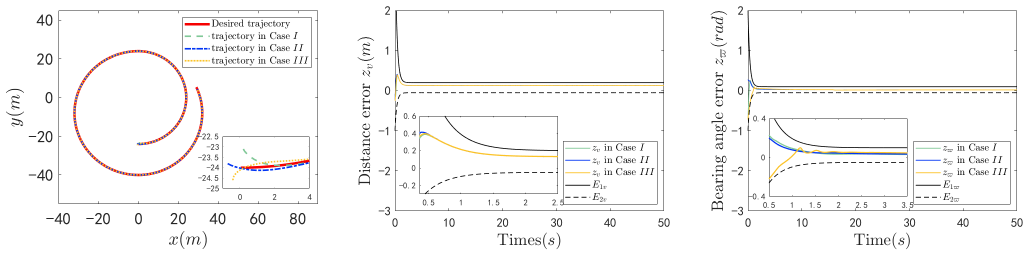

(**a**) output trajectory (**b**) tracking error z_v (**c**) tracking error z_ω

Figure 6. The tracking effect comparison of Example 2 among Cases *I*, *II*, and *III*.

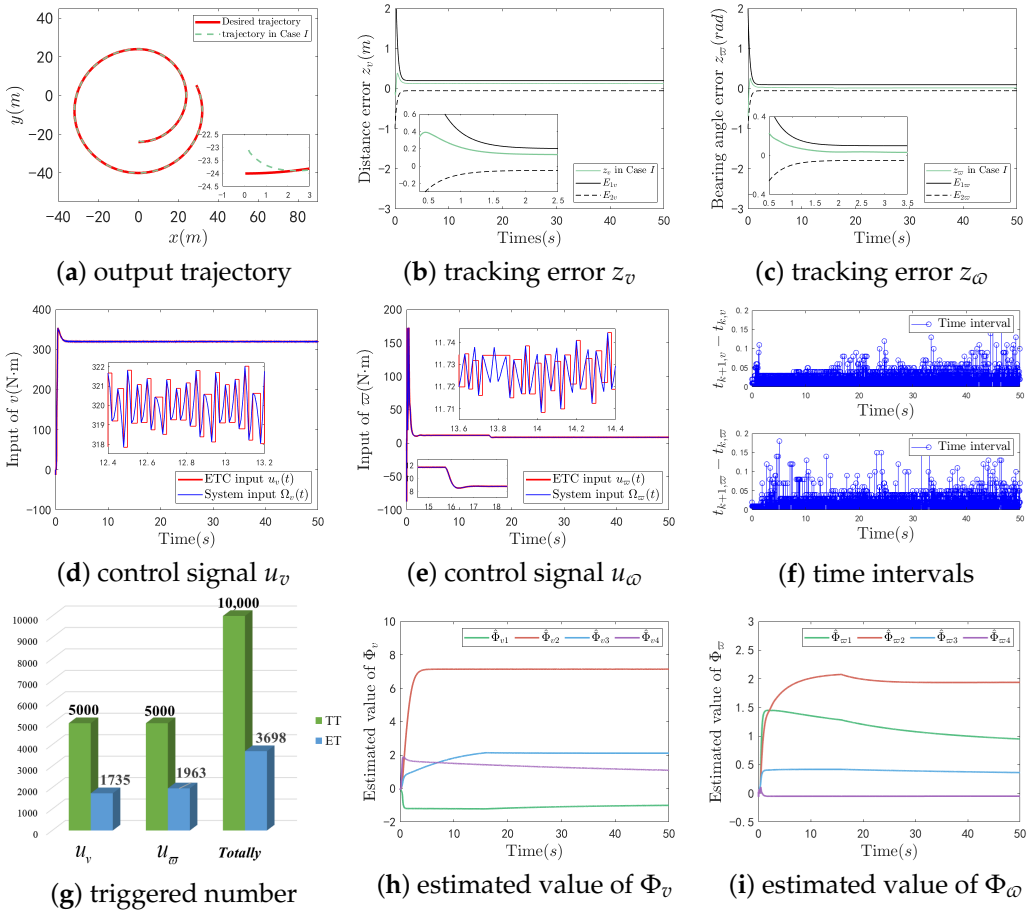

(**a**) output trajectory (**b**) tracking error z_v (**c**) tracking error z_ω

(**d**) control signal u_v (**e**) control signal u_ω (**f**) time intervals

(**g**) triggered number (**h**) estimated value of Φ_v (**i**) estimated value of Φ_ω

Figure 7. The simulation results of Example 2 in Case *I*.

Table 5. NMR initial conditions in Example 2.

State	$x(0)$	$y(0)$	$\phi(0)$	$v(0)$	$\varpi(0)$
I	0.2 [m]	−23.1 [m]	$-\frac{\pi}{3}$ [rad]	2.3 [m/s]	1.0 [rad/s]
II	−0.7 [m]	−23.8 [m]	$-\frac{\pi}{6}$ [rad]	3.0 [m/s]	1.5 [rad/s]
III	−0.4 [m]	−24.6 [m]	$\frac{\pi}{2}$ [rad]	3.5 [m/s]	2.0 [rad/s]

Table 6. The specified parameters and the controller parameters of Example 2.

The parameters of relative posture	$E_{1v} = 1.2\,[\mathrm{m}]$, $E_{2v} = 0.95\,[\mathrm{m}]$, $E_{1\omega} = 0.1\,[\mathrm{rad}]$, $E_{2\omega} = -0.05\,[\mathrm{rad}]$, $\bar{E}_v = 1\,[\mathrm{m}]$, $\bar{E}_\omega = 0\,[\mathrm{rad}]$.
The parameters of controllers	$\xi = 68/101$, $k_{11v} = k_{21v} = 60$, $k_{12v} = k_{22v} = 4$, $k_{11\omega} = k_{21\omega} = 42$, $k_{12\omega} = k_{22\omega} = 3$, $f_v = 1.2$, $f_\omega = 1.4$, $\eta_{v,1} = \eta_{v,2} = 0.6$, $\eta_{\omega,1} = \eta_{\omega,2} = 1.7$, $\kappa_v = h_v = 0.1$, $\kappa_\omega = h_\omega = 0.1$, $\mathrm{K}_v = diag(0.1, 0.1, 0.1, 0.03)$, $\mathrm{K}_\omega = diag(0.1, 0.1, 0.1, 0.01)$, $\hat{\Phi}_v(0) = \hat{\Phi}_\omega(0) = [0, 0, 0, 0]^T$.
The parameters of PPF	$B_{1v} = (1 - 0.2)e^{-0.33t} + 0.2$, $B_{2v} = (1 - 0.05)e^{-0.33t} + 0.05$, $B_{1\omega} = (1 - 0.1)e^{-0.33t} + 0.1$, $B_{2\omega} = (1 - 0.05)e^{-0.33t} + 0.05$, $\chi_v = \chi_\omega = 3$, $Q_v = Q_\omega = 20$, $\bar{\lambda}_v = 4$, $\lambda_v = 1$,$\bar{\lambda}_\omega = 2$, $\lambda_\omega = 1$.
The parameter of ETM	$\vartheta_v = 2$, $\vartheta_\omega = 2$, $\sigma_v = 0.005$, $\sigma_\omega = 0.001$, $g_v = 0.015$, $g_\omega = 0.01$.

Table 7. Triggered number of Example II in Case I.

Triggered Number / **Object** / **Scheme**	u_v	u_ω	**Total**
Time-Triggered Scheme	5000	5000	10,000
Event-Triggered Scheme	1735	1963	3698
The Rate	65.300%	60.740%	63.020%

In the actual application process of the NMR, the wheels tend to be affected by road conditions, which would lead to various deformation of the wheels, and then the radius of the wheels would correspondingly change. Therefore, a deformation disturbance signal of the radius of wheels is introduced into Example 2 to further simulate the actual application process of the NMR under wheel deformation. As shown in Figure 8a, the elements of signal are randomly selected from the range $[0.12, 0.18]$.

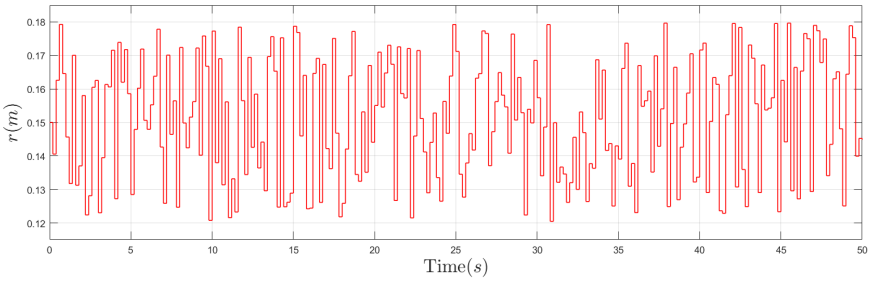

(**a**) deformation disturbances signal of the radius of wheels

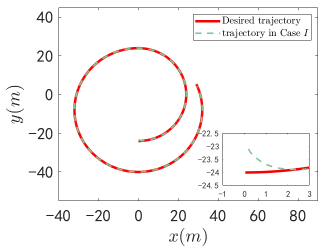

(**b**) output trajectory

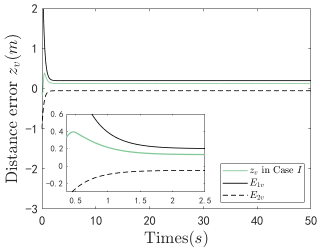

(**c**) tracking error z_v

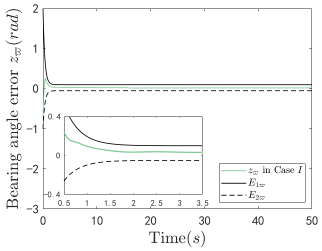

(**d**) tracking error z_ω

Figure 8. *Cont.*

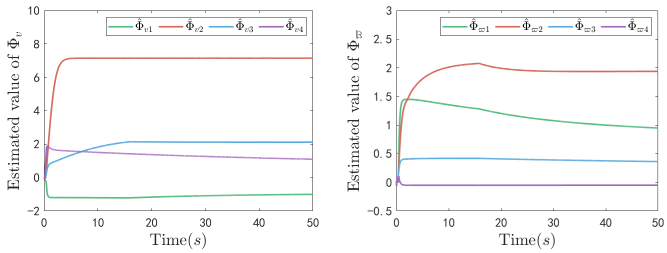

(**e**) estimated value of Φ_ω (**f**) estimated value of Φ_ω

Figure 8. The tracking effect of Example 2 under disturbances of r in Case I.

From Figure 8, it can be seen that the NMR can attain the desired performance in a dislodging mission under deformation disturbances of the radius of the wheels, showing nice robustness of the proposed control strategy.

4.3. Comparison with Related Work

As shown in Table 8, in comparison with related research in the literature, it can be seen that the majority of these studies focused more on Lyapunov asymptotic or finite-time control framework. The fixed-time framework can render the convergence time independent of initial conditions of the system and greatly enhance the adaptability for practical applications. Similar to the purpose of fixed-time control, ETM, asymmetric state constraints and utilizing torque as an input signal can contribute to improving the practicability or adaptability of the proposed method for NMRs. Moreover, prescribed performance can even maintain the tracking errors of the system being limited in a given region so as to effectively avoid collision or losing visibility with the enemy.

Table 8. Comparison with related work.

Scheme	Convergence Framework	Triggered Strategy	Sate Constraint	Input Signal	Prescribed Performance
In [20]	Finite-T	TT	Sym	Torque	NO
In [32]	AS	ET	Sym	Torque	NO
In [33]	AS	ET	Sym	Velocity	NO
In [34]	AS	TT	Sym	Torque	YES
In [37]	Fixed-T	TT	Sym	Torque	YES
In [38]	Finite-T	TT	Sym	Velocity	NO
Proposed	Fixed-T	ET	Asym	Torque	YES

AS = Asymptotic Stability, Fixed-T = Fixed-Time, Finite-T = Finite-Time, ET = Event-Triggered, TT = Time-Triggered, Sym = Symmetric, Asym = Asymmetric.

4.4. Discussion

From the above analysis and experimental results, it can be seen that the NMR system could implement the dislodging mission and perform high precision tracking. Additionally, similar to the theoretical deduction, the system is capable of achieving fixed-time convergence while the transient and steady-state performance are guaranteed. Therefore, collision between the enemy robot and the manipulated robot is effectively avoided, and the manipulated robot can always maintain the visibility of the enemy while implementing the dislodging mission. In addition, the convergence time is independent of the initial conditions, showing great scalability and universality of the system. Moreover, the burden of the controller-to-actuator channel is effectively alleviated by utilizing ETM with a relative threshold. At least 63.020% of communication resources are well preserved.

Nevertheless, if the triggered condition of the ETM with relative threshold is satisfied, it can be understood that the ETM would be triggered and the ETC input signal would be updated. Consequently, when the control signal abruptly surges, the system would suffer a significant impulse, which may deteriorate the system performance. This can be seen in Figures 3e and 7e. Therefore, a prescribed performance function is introduced to restrict the tracking errors z_v and z_ω in a given region, so as to diminish the impact caused by abrupt significant control signals. It can be also seen from Figures 3b,c and 7b,c that the trajectories of the tracking errors can be effectively maintained in the prescribed region while the control signals are relatively large.

5. Conclusions

In this research, a fixed-time guaranteed performance adaptive event-triggered tracking control method has been investigated for a category of NMRs under asymmetric state constraints. By taking a backstepping technique as backbone, an ABLF is constructed to ensure the tracking errors converge with a predefined time that is irrelevant to the initial conditions of the system, and the violation of asymmetric constraints is effectively avoided. Additionally, a transform function is formulated to guarantee the transient and steady-state performance of the tracking errors. Specifically, the NMR is capable of showing great tracking performance since the collision between enemy robot and NMR is avoided throughout the dislodging mission and the NMR never loses the visibility of the enemy. In addition, an ETM with relative threshold is introduced to preserve communication bandwidth from the controller to the actuator, and Zeno behavior is successfully eliminated. Ultimately, two simulation results are carried out to verify the validity of the proposed control strategy. In future work, how to develop an ETM that could prevent significant impulse input from being introduced into the system and place that ETM into the sensor-to-controller channel will be our area of interest.

Author Contributions: Data curation, W.H.; Investigation, Y.G. and Z.Z.; Methodology, K.C.; Project administration, X.W.; Software, W.H. and Z.W.; Supervision, Z.W.; Validation, Y.G., Z.Z., Z.W. and X.W.; Visualization, Z.Z.; Writing—original draft, K.C. and Y.G.; Writing—review and editing, K.C., Y.G., W.H. and X.W. All authors have read and agreed to the published version of the manuscript.

Funding: This work was funded by the National Natural Science Foundation of China under Grant 62103115, in part of the Science and Technology Research Program of Guangzhou under Grant 2024A04J9895 and in part of the Special Funds for the Cultivation of Guangdong College Student's Scientific and the Technological Innovation under Grant pdjh2024a297.

Data Availability Statement: All relevant data are within the paper.

Conflicts of Interest: The authors declare no conflicts of interest.

References

1. Li, X.; Li, Z.; Wang, H.; Li, W. Unmanned Aerial Vehicle for Transmission Line Inspection: Status, Standardization, and Perspectives. *Front. Energy Res.* **2021**, *9*, 713634. [CrossRef]
2. Mu, J.; Zhang, R.; Cui, Y.; Gao, N.; Jing, X. UAV Meets Integrated Sensing and Communication: Challenges and Future Directions. *IEEE Commun. Mag.* **2023**, *61*, 62–67. [CrossRef]
3. Zhang, Z.; Xu, Y.; Wan, L.; Chen, G.; Cao, Y. Rotation matrix-based finite-time trajectory tracking control of AUV with output constraints and input quantization. *Ocean Eng.* **2024**, *293*, 116570. [CrossRef]
4. Anil, B.; Sneha, G. Optimal tracking control of an Autonomous Underwater Vehicle: A PMP approach. *ISA Trans.* **2024**, *145*, 298–314.
5. Kourosh, D.; Luigi, P.; Joao, R.; Rafael, C.; Jerry, P.; Eiichi, Y.; Serena, I.; Daniele, P. Teleoperation of Humanoid Robots: A Survey. *IEEE Trans. Rob.* **2023**, *39*, 1706–1727.
6. Tomoki, A.; Seppelfelt, G.D.C.; Takayuki, N.; Soh, Y. HumanoidBot: Framework for integrating full-body humanoid robot with open-domain chat system. *Adv. Rob.* **2023**, *37*, 1171–1186.
7. Huang, Y.; Su, J. Visual Servoing of Nonholonomic Mobile Robots: A Review and a Novel Perspective. *IEEE Access* **2019**, *7*, 134968–134977. [CrossRef]
8. Jose, G.R.; Emmanuel, N.; Esteban, R.; Rafael, C.; Marco, M. A Smooth Time–Varying PID Controller for Nonholonomic Mobile Robots Subject to Matched Disturbances. *J. Intell. Robot. Syst.* **2022**, *105*, 13.

9. Guadalupe, R.J.; David, N.A.; Emmanuel, N.; Que, H. A Globally Convergent Adaptive Velocity Observer for Nonholonomic Mobile Robots Affected by Unknown Disturbances. *IEEE Control Syst. Lett.* **2022**, *7*, 85–90.
10. Liu, M.; Wu, K.; Wu, Y. Finite-time tracking control of disturbed non-holonomic systems with input saturation and state constraints: Theory and experiment. *IET Control. Theory Appl.* **2023**, *17*, 1663–1676. [CrossRef]
11. Zhang, J.; Fang, Z.; Zhang, Z.; Gao, R.; Zhang, S. Trajectory Tracking Control of Nonholonomic Wheeled Mobile Robots Using Model Predictive Control Subjected to Lyapunov-based Input Constraints. *Int. J. Control Autom.* **2022**, *20*, 1640–1651. [CrossRef]
12. Xie, H.; Zheng, J.; Sun, Z.; Wang, H.; Chai, R. Finite-time tracking control for nonholonomic wheeled mobile robot using adaptive fast nonsingular terminal sliding mode. *Nonlinear Dyn.* **2022**, *110*, 1437–1453. [CrossRef]
13. Shi, S.; Xu, S.; Yu, X.; Li, Y.; Zhang, Z. Finite-time tracking control of uncertain nonholonomic systems by state and output feedback. *Int. J. Robust Nonlinear Control* **2018**, *28*, 1942–1959. [CrossRef]
14. Fu, J.; Tian, F.; Chai, T.; Jing, Y.; Li, Z.; Su, C. Motion Tracking Control Design for a Class of Nonholonomic Mobile Robot Systems. *IEEE Trans. Syst. Man Cybern.* **2020**, *50*, 2150–2156. [CrossRef]
15. Li, J. Adaptive Tracking and Stabilization of Nonholonomic Mobile Robots with Input Saturation. *IEEE Trans. Autom. Control* **2022**, *67*, 6173–6179. [CrossRef]
16. Lu, K.; Dai, S.; Jin, X. Fixed-Time Rigidity-Based Formation Maneuvering for Nonholonomic Multirobot Systems with Prescribed Performance. *IEEE Trans. Cybern.* **2022**, *54*, 2129–2141. [CrossRef]
17. Dai, S.; Lu, K.; Fu, J. Adaptive Finite-Time Tracking Control of Nonholonomic Multirobot Formation Systems with Limited Field-of-View Sensors. *IEEE Trans. Cybern.* **2022**, *52*, 10695–10708. [CrossRef] [PubMed]
18. Jhang, J.; Wu, J.; Yung, C. Stabilization of Nonlinear Control-Affine Systems with Multiple State Constraints. *IEEE Access* **2022**, *8*, 179735–179744. [CrossRef]
19. Wang, X.; Pang, N.; Xu, Y.; Huang, T.; Jurgen, K. On State-Constrained Containment Control for Nonlinear Multiagent Systems Using Event-Triggered Input. *IEEE Trans. Syst. Man Cybern.* **2024**. [CrossRef]
20. Kong, L.; Yu, X.; Zhang, S. Neuro-learning-based adaptive control for state-constrained strict-feedback systems with unknown control direction. *ISA Trans.* **2021**, *112*, 12–22. [CrossRef]
21. Guo, Y.; Xu, B.; Han, W.; Li, S.; Wang, Y.; Zhang, Y. Robust adaptive control of hypersonic flight vehicle with asymmetric AOA constraint. *Sci. China Inform. Sci.* **2020**, *63*, 212203. [CrossRef]
22. Wang, C.; Wang, J.; Zhang, C.; Du, Y.; Liu, Z.; Chen, C. Fixed-time event-triggered consensus tracking control for uncertain nonlinear multiagent systems with dead-zone constraint. *Int. J. Robust Nonlinear Control* **2023**, *33*, 6151–6170. [CrossRef]
23. Li, Y.; Zhu, L.; Guo, Y. Observer-based multivariable fixed-time formation control of mobile robots. *J. Syst. Eng. Electron.* **2020**, *31*, 403–414. [CrossRef]
24. Sun, F.; Li, H.; Zhu, W.; Juergen, K. Fixed-time formation tracking for multiple nonholonomic wheeled mobile robots based on distributed observer. *Nonlinear Dyn.* **2021**, *106*, 3331–3349. [CrossRef]
25. Zhu, Z.; Yin, Y.; Wang, F.; Liu, Z.; Chen, Z. Practical robust fixed-time containment control for multi-agent systems under actuator faults. *Expert Syst. Appl.* **2024**, *245*, 123152. [CrossRef]
26. Cui, L.; Jin, N.; Chang, S.; Zuo, Z.; Zhao, Z. Fixed-time ESO based fixed-time integral terminal sliding mode controller design for a missile. *ISA Trans.* **2022**, *125*, 237–251. [CrossRef] [PubMed]
27. Yang, C.; Hu, G.; Song, Q.; Wang, Y.; Yang, W. Fixed-Time Sliding Mode Control for Linear Motor Traction Systems with Prescribed Performance. *Energies* **2024**, *17*, 952. [CrossRef]
28. Chen, K.; Yan, C.; Ren, Q.; Wang, J. Dynamic event-triggered leader-following consensus of nonlinear multi-agent systems with measurement noises. *IET Control. Theory Appl.* **2023**, *17*, 1367–1380. [CrossRef]
29. Cheng, G.; Kong, L.; Niu, W.; Wu, Y.; Arif, M.M. Fixed-Time Event-Triggered Control for a Building-like Structure with Prescribed Performance. *IEEE Trans. Syst. Man Cybern. Syst.* **2024**, *54*, 2711–2722. [CrossRef]
30. Kang, W.; Liu, C. Event-triggered stabilization for large-scale interconnected systems with time delays. *Int. J. Robust Nonlinear Control* **2022**, *32*, 7469–7487. [CrossRef]
31. Yoo, J.; Johansson, K.H. Event-Triggered Model Predictive Control with a Statistical Learning. *IEEE Trans. Syst. Man, Cybern. Syst.* **2021**, *51*, 2571–2581. [CrossRef]
32. Sami, A.I.; Arghya, C.; Indrani, K. Adaptive Control of a Networked Mobile Robot Subject to Parameter Uncertainties and Limited Communications. In Proceedings of the 2019 Sixth Indian Control Conference (ICC), Hyderabad, Indonesia, 18–20 December 2019.
33. Sami, A.I.; Indrani, K. Design and implementation of event-triggered adaptive controller for commercial mobile robots subject to input delays and limited communications. *Control Eng. Pract.* **2021**, *114*, 104865.
34. Dai, S.; De, S.; Chen, X.; Jin, X. Adaptive Leader-Follower Formation Control of Nonholonomic Mobile Robots with Prescribed Transient and Steady-State Performance. *IEEE Trans. Ind. Inf.* **2020**, *16*, 3662–3671. [CrossRef]
35. Yue, X.; Liu, J.; Chen, K.; Zhang, Y.; Hu, Z. Prescribed performance adaptive event-triggered consensus control for multiagent systems with input saturation. *Front. Neurorob.* **2023**, *16*, 1103462. [CrossRef] [PubMed]
36. Zhang, L.; Guo, Y.; Hua, C. Adaptive Event-triggered Control for High-order Nonlinear Systems with Deferred Asymmetric Full-state Constraints. *Int. J. Control. Autom. Syst.* **2023**, *21*, 2183–2190. [CrossRef]

37. Dai, S.; Lu, K.; Xu, J. Fixed-Time Formation Control of Unicycle-Type Mobile Robots with Visibility and Performance Constraints. *IEEE Trans. Ind. Electron.* **2021**, *68*, 12615–12625. [CrossRef]
38. Miranda-Colorado, R. Observer-based finite-time control for trajectory tracking of wheeled mobile robots with kinematic disturbances. *ISA Trans.* 2024, *ahead of print*. [CrossRef]